Measuring the Elastic Modulus of Thin Films by Capillary Wrinkling Annuli

Stuart Poole

May 16, 2017

Abstract

A floated annulus subject to a difference in surface tension between the inside and outside edges will deform under the stress. The form of this deformation is a predictable wrinkling pattern which has been observed previously by Farmer[1]. Farmer wrinkled some thin film annuli and attempted to calculate the elastic modulus from the number of wrinkles formed. His results were larger by a factor of 10 to the expected value of $E_{\text{polystyrene}} = 3.2 - 3.4\text{GPa}$[2]. The previous model for the wrinkling ignored the component of buckling in the radial direction and used mathematics intended for a plane strain problem. Capillary wrinkling the annuli is an example of a plane stress problem so required adjustment. The lighting used previously was flat and did not highlight the wrinkling behaviour effectively so an investigation into improving the image quality was conducted. This paper illustrates the implications of measuring the elastic modulus of a thin film and describes the various mathematical models of the buckling. A reproduction of Farmer's result was done before the model was adjusted to account for radial buckling and conversion to a plane stress problem. The aim was to improve the model and to allow for the measurement of the elastic modulus of ultra-thin films. This would allow for free surface material properties to be measured for polymers. The elastic modulus was measured for polystyrene films in the $80 - 90$ nm range and were found within a factor of 4 indicating that the method is plausible. If the model can be improved and the measurement can be conducted in a more isolated environment it is likely to be an effective method for measuring the elastic modulus of an ultra-thin film.

Contents

1 Introduction

Polymer films are widely used in many products and research applications. Common uses include packaging purposes such as using cling film (either PVC or LDPE+LLDPE films with thickness $h \sim 10 - 100$ µm)[3] as well as having widespread applications in medical and contraceptive devices, sterile gloves and condoms as respective examples. Many protective coatings on machinery and military vehicles use a polyurethane based coating which has been developed to withstand punishment[4]. Thin film coatings can also be used to provide desired wetting or optical properties such as hydrophobic behaviour and anti-reflection[5]. The cosmetics industry is interested in measuring the material properties of thin films, especially in wrinkling, because the models can be used to predict the movement of skin or how the make-up will react to the changes of the skin when smiling, for example. This report will describe the wrinkling thin films to observe the elastic properties of the material. Mathematical models of the wrinkling will be derived in order to predict the form, the result of which may be useful for other applications. The report will describe the attempt to convert the number of wrinkles into a measure of the elastic modulus of the film.

A free surface is any surface that is not in contact with the bulk of the structure. In polymers, these surfaces act differently to the bulk of the material due to differences in the local environment, specifically, surface polymer chains are more tightly bound. These differences penetrate only the first few layers and have effects on the material properties of the free surfaces. As an example, the glass transition temperature is reduced in free surfaces[6]. This and several other phenomena have been investigated and research is ongoing with the aims of understanding more of the differences[7]. If the thickness of a film is reduced so that they become ultra-thin films, that is to approach the length scale of the polymer chains themselves, the material will exhibit the properties of the free surfaces instead of the bulk. Measurements of ultra-thin films can be used to determine the properties of the free surfaces.

A previous attempt to easily measure the elastic modulus (Young's modulus) of an ultra-thin film was made by Farmer[1]. That experiment used capillary forces to wrinkle an annulus of a thin film. A count of the number of wrinkles was used in conjunction with a mathematical model to determine an estimate of the elastic modulus of the film. The overall aim was to develop a technique to measure the elastic modulus of thin films. The thesis concluded that the experiment was unsuccessful because the model did not account for all forms of bending[1]. The count of wrinkles was also not reliable enough. This was due to low contrast between peaks and troughs in the images. It was suggested that the wrinkling behaviour and counting of wrinkles could be a plausible method if the issues were overcome.

If the mathematical model can be derived to account for radial bending, and improvements to the lighting can be made then it may be possible to produce a realistic value for the elastic modulus. The technique and model, if reliable, provides a reproducible and readily available way to measure the elastic properties of ultra-thin films; the most specialist piece of equipment required is a Langmuir-Blodgett trough which is common in polymer laboratories. The other notable equipment including a diffuse light source, such as an LED panel, and a still image camera, preferably with manual aperture and focus, are also readily available. Using these tools in conjunction with some black objects and a piece of plane white paper, images with high enough quality to measure the elastic modulus can be obtained. The images are taken of a wrinkled thin film annulus subject to a range of capillary force magnitudes and an automated count of wrinkles is performed on each.

This report aims to investigate the viability of the technique by deriving a new model and investigating the possibility of lighting the annulus to clearly expose the wrinkles in the image. The report includes an overview of the physics required to understand the problem, a description

of the new mathematical models that were derived; an explanation of the experimental methods used; a discussion of the results and their implications; a discussion of the limits of the technique; and finally, a summary and set of conclusions. The viability and reliability of the technique will be evaluated and some suggestions for improvements and any further investigations are made.

2 Theory

Before describing the experimental techniques, some key physical concepts need to be understood. These concepts are the basics of polymer physics and the effect free surfaces have on properties of the polymer structures; what surfactants are and how they affect surface tensions; how spin coating works and how it can be used to make thin films; how the thickness of a thin film can be measured using ellipsometry; the forces that act on an annulus of a thin film floated on water and how a surfactant can be used to cause wrinkling; and how the resulting wrinkling can be used to determine the elastic modulus of the material that makes up the annulus.

The word polymer stems from the Greek words for many and parts[8]. Polymers are long chains of smaller molecules (monomers) that join together. These chains coil up and intertwine forming complex mats of chains. The length of the chains can range significantly, however for a given polymer the average length can be determined and the result is called the root mean square end to end distance (RMS e-e distance). The structure of the polymer at the surfaces is different to bulk, in particular the polymer chains pack more tightly to reduce the entropy losses to the surface interface. The material will only exhibit this free surface behaviour for a few lengths of the polymer, such that only a few surface layers will be affected[9, 10, 7].

In following experiment polystyrene was used which has a RMS e-e distance of $R_{\text{rms}} = 20$ nm[11]. This means that the free surface effects spread to a thickness a few times this length. Because the aim is to verify that the technique can be used to measure the elastic modulus, relatively thick films will be used so that the material exhibits known behaviours. This requires the thicknesses to be $h > 3R_{\text{rms}} \sim 60$ nm therefore thicknesses of $h \sim 90$ nm are used to be sure.

Surfactants (surface acting agents) are lipids which reduce the surface tension of a liquid when added. They typically contain a hydrophilic head group and hydrophobic tail group which act to to form micelles, liposomes or bilayer sheets. A bilayer sheet will form on surfaces to reduce the amount of contact the surfactant molecules have with the liquid to minimise energy. These bilayers cover the full surface of the liquid with excess molecules forming micelles or liposomes in suspension. Because the bilayer on the surface is formed by a lipid with weaker intermolecular forces than water, the surface bilayer will exhibit reduced surface tension if the liquid is water. Thus the concentration of surfactant can be used to control the surface tension of a water-air interface[12].

If a polymer film is floated on a water sub-phase, the surface of the water will apply tension to the side faces of the film. The magnitude is determined by the surface tension of the water. This tension does not act uniformly across the side face of the film but instead wetting effects cause the tension to be applied non-uniformly[13]. The exact form the this wetting is hard to cahracterise and would complicated the model unnecessarily. For thin films it can be assumed that the force is uniformly distributed because the length of the wetting effects are small. This allows the surface tension to be considered as a pressure acting on the side of the film, with magnitude equal to

$$\sigma = \frac{\gamma}{h} \tag{1}$$

where σ is the pressure, γ is the surface tension and h is the thickness of the film.

Dissolving a polymer in solvent allows for a small mass of polymer to be evenly distributed in a large volume. Having a low density of polymer allows for a droplet to be placed on a plate. Spinning the plate will spread the polymer thinly and allow the solvent to evaporate, leaving a thin film of polymer deposited on the plate. This is the essence of spin coating and is used to generate the thin films used in this experiment. The thickness of the film depends on many factors but the easiest to control are the rate of rotation and concentration of polymer in the solvent. Spinning the plate at higher rate applies more radial force and so spreads the polymer thinner. In contrast, having a higher concentration of polymer in the solvent means that more polymer will be deposited under the same conditions. These two factors makes it easy to control the thickness of polymer films in spin coating. Annuli can be cut easily by pressing a sharp tool into the polymer while it is spinning. This is done twice to make two circular cuts centred on the axis of rotation such that an annulus is drawn.

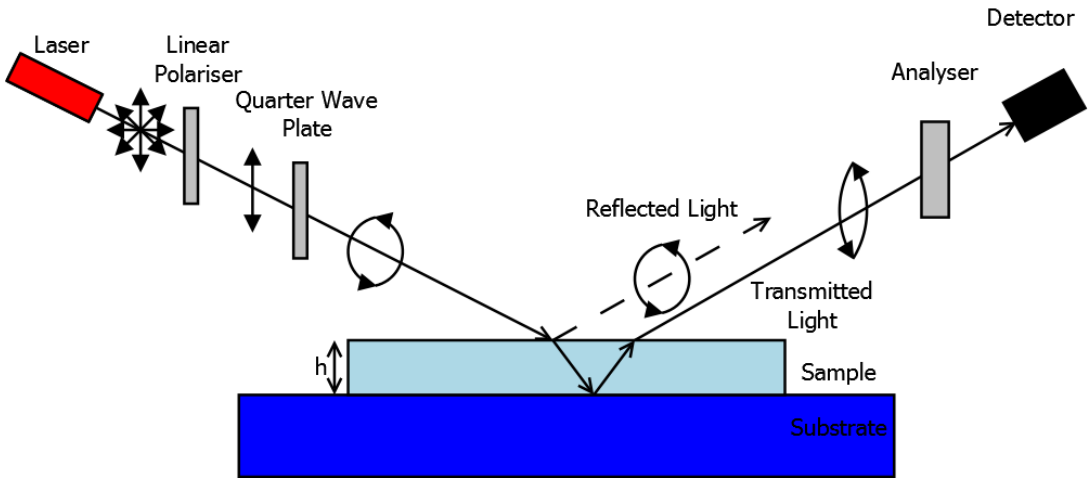

Figure 1: A schematic diagram of the optical arrangement used in null ellipsometry when measuring the thickness of a thin film. The aim is to reduce the reflected light to zero by adjusting the incident angle and to adjust the orientations of the polariser, quarter wave plate and the analyser to measure a zero intensity of light in the detector. There are four different combinations of angles to result in zero intensity so they are all considered.

Null ellipsometry is a technique which allows the thickness of a film to be determined by finding the change in polarisation caused by light passing through a film at an angle. The optical arrangement required is displayed in Fig. 1 and shows that the light from a laser source is first linearly polarised before it is elliptically polarised with a quarter wave plate (compensator). This elliptically polarised light illuminates the sample which rests on a reflective substrate (silicon) such that some light is reflected off the sample surface and some is transmitted through the film and reflected off the substrate.[14] If the the incident angle is set to the polarisation angle of the sample material then the reflected light should be eliminated leaving only the transmitted light[15]. Passing through the sample affects the polarisation of the transmitted light such that the thickness can be determined by how much the polarisation has changed. In null ellipsometry the orientations of the compensator, linear polariser and analyser are adjusted until the detected intensity is zero, such that the light is nulled. The nulling occurs when the elliptically polarised light becomes perfectly linear after passing through the sample. The analyser can then be aligned perpendicular to the polarisation such that it exactly cancels the light. The angles required for the nulling are used to calculate the thickness of the film[16].

If an annulus is floated onto water so that the enclosed area contains pure water, surfactant

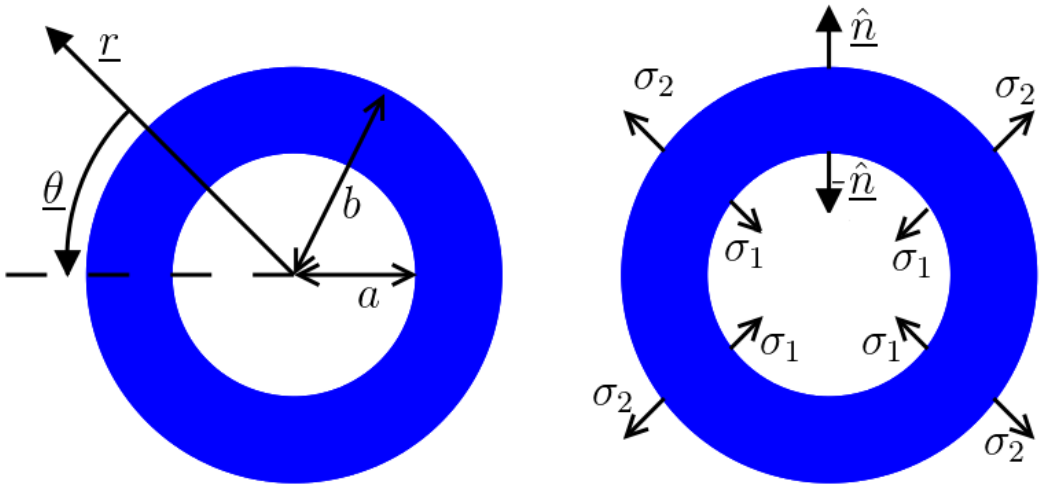

Figure 2: An illustration of unit vectors and forces acting on the annuli used in this model.

can be added around the outside of the annulus. This will cause a difference in surface tensions effectively compressing the annulus. This allows the forces to be considered as a plane stress problem i.e. a problem in which the stresses only act in the plane of a plate. Previously it was treated as a plane strain problem i.e. a problem in which the displacement is only in the planar directions[1, 17]. Luckily it is simple to convert one to the other. Cylindrical polar coordinates are chosen since the coordinates reflect the symmetry of the problem. The forces, sizes and directions are illustrated in Fig. 2. The forces acting on the inside and outside faces are considered as pressures σ_1 and σ_2 respectively. These act on the surface at $r = a$ and $r = b$. This causes the annulus to wrinkle out of the plane of the annulus. The forces cause a small change in the sizes a and b, but these are so small that they cannot be measured and therefore the contribution to energy is negligible. First the previous maths will be worked through with corrections, and then the derivation will be adjusted by using both the equivalence of plane stress and plane strain and an additional term in the form of buckling i.e. accounting for the radial bending.

An annulus is floated on pure water and surfactant is applied outside the annulus. The concentration of the surfactant can then be altered by changing the area it occupies. Assuming that the surfactant remains in the surface bilayer phase, the surface tension inside the annulus should remain pure water, with surface tension γ_1, which acts inwards. The surfactant acts to reduce the surface tension outside of the annulus, γ_2, which acts outwards. The result is a larger force acting inwards than outwards and results in an annulus under tension. Ultimately the radii of the inner and outer edges are reduced and so the annulus is compressed. The difference in surface tensions can also be expressed as a difference in surface pressures, where the difference in tensions is also (somewhat confusingly) referred to as the surface pressure, Π. The relation is given by

$$\Pi = h(\sigma_1 - \sigma_2) = \gamma_1 - \gamma_2 \tag{2}$$

where h is the thickness of the film.

Using expressions for the forces applied, the energies stored in the annulus and the work done in bending the annulus can be combined to find the total energy of the system. Finding a minimum energy as a function of number of wrinkles will allow the equilibrium number of wrinkles to be determined. A general set of equilibrium equations were used to derive the form of radial displacement field which allowed the forms of the stress fields to be determined from known boundary conditions (the pressures applied to the edge faces of the annulus). The stress

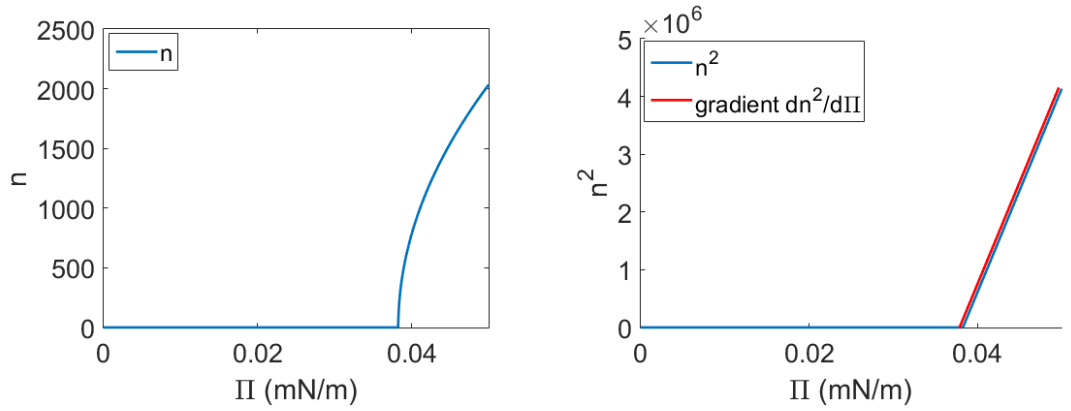

(a) Example plot of n as a function of Π to illustrate the square root dependence above the nucleation point.

(b) Example plot of n^2 as a function of Π. This illustrates the linearly dependence of the plot above a nucleation point, and highlights the gradient that is used to calculate the elastic modulus.

Figure 3: Plots to show the form of the growth of wrinkles predicted by the model.

fields are required to calculate the work done by the forces. Usually the form of the vertical displacement field is derived from first principles but in this report the forms were assumed, and compared to the observed wrinkling. The result of the derivation showed that the square of the number of wrinkles is linearly dependant on the surface pressure difference Π in all four expressions. The dependence is demonstrated in Fig. 3. Taking the gradient gives a result that allows the elastic modulus to be calculated using the shape of the annulus, the Poisson ratio and the gradient, $\frac{dn^2}{d\Pi}$, illustrated in Fig. 3b. This allows the elastic modulus to be calculated if the Poisson ratio is known and visa versa. Two forms of wrinkling are considered and both a plane stress and a plane strain approach is used. This leads to four different values of the elastic modulus per annulus. The full derivation of the expressions is included in Appendix A for those interested. Part of Appendix A contains the constant, F, which will be used here too. F is a shorthand for the sum of several constants which are functions of the Poisson Ratio, ν. It comes from the conversion from a plane strain to a plane stress problem. The exact form of$F$ is given below:

$$F = \frac{2\nu}{1-2\nu} + \frac{2}{\frac{\nu}{1-2\nu}+1} - \frac{1}{\frac{\nu}{1-2\nu}+\frac{1}{2}} \tag{3}$$

First the form of wrinkling which only depends on the angle will be considered. The form of this bending is described by

$$w_{simple} = w_0 \cos(n\theta) \tag{4}$$

where w_0 is the amplitude of the bending. This form of bending is illustrated in Fig. 4. This form of bending gives the equations for the elastic modulus described by the growth of wrinkles given by

$$E_{\text{simple, strain}} = \frac{-12(1-\nu^2)}{\left(\frac{dn^2}{d\Pi}\right)h^3}\left(\frac{a^2b^2}{a^2-b^2}\right)\left\{\frac{b^2\ln\left(\frac{b}{a}\right)}{b^2-a^2}+\frac{1}{2}\right\} \tag{5}$$

$$E_{\text{simple, stress}} = \frac{-12\left(1-\left(\frac{\nu}{1+\nu}\right)^2\right)(1+\nu)^2}{\left(\frac{dn^2}{d\Pi}\right)h^3(1+2\nu)}\left(\frac{a^2b^2}{a^2-b^2}\right)\left\{\frac{b^2\ln\left(\frac{b}{a}\right)}{b^2-a^2}F+\frac{1}{2}\right\} \tag{6}$$

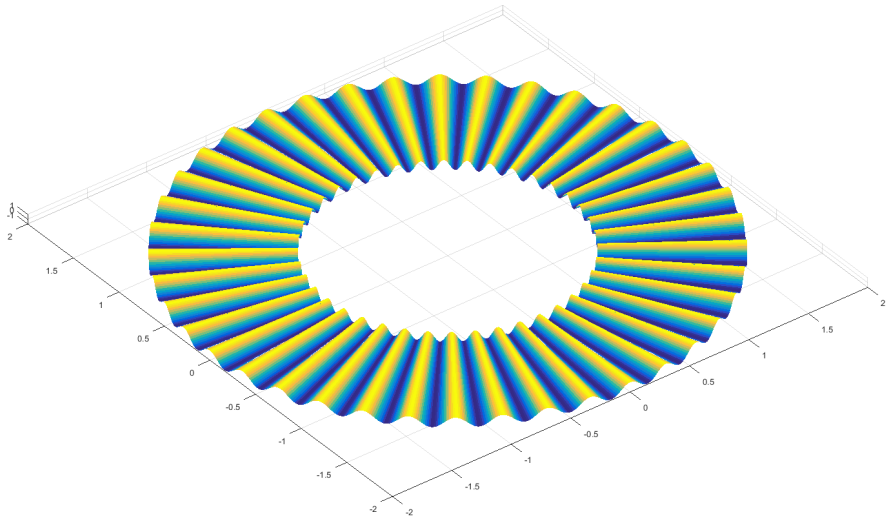

Figure 4: The simplified form of wrinkling which ignores any radial dependence. The wrinkling is portrayed in the r-z plane.

The simple form of wrinkling does not accurately describe the observed shape of the wrinkles since the edges of the annulus are pinned to the surface of the water by the surface pressures. A suggested form of wrinkling for the observed shape is described by

$$w_{radial} = w_0\cos(n\theta)\sin\left(\frac{\pi(r-a)}{(b-a)}\right) \tag{7}$$

and gives the form illustrated in Fig. 5. From the figure it is is clear to see that the annulus is pinned at the edges. This form of bending results in a much more complicated expression for the energies but still simplifies to the manageable expressions below:

$$E_{\text{radial, strain}} = \frac{-6(1-\nu^2)b^2}{\left(\frac{dn^2}{d\Pi}\right)h^3(a^2-b^2)}\left\{\frac{\int_a^b \frac{\sin^2\left(\frac{\pi(r-a)}{(b-a)}\right)}{r}dr}{\int_a^b \frac{\sin^2\left(\frac{\pi(r-a)}{(b-a)}\right)}{r^3}dr}+a^2\right\} \tag{8}$$

$$E_{\text{radial, stress}} = \frac{-6\left(1-\left(\frac{\nu}{1+\nu}\right)^2\right)(1+\nu)^2b^2}{\left(\frac{dn^2}{d\Pi}\right)h^3(1+2\nu)(a^2-b^2)}\left\{\frac{\int_a^b \frac{\sin^2\left(\frac{\pi(r-a)}{(b-a)}\right)}{r}dr}{\int_a^b \frac{\sin^2\left(\frac{\pi(r-a)}{(b-a)}\right)}{r^3}dr}+a^2F\right\} \tag{9}$$

To test the models, we compared the intercept of fit to the linear section to the predicted nucleation point, Π_{nuc}, determined from the energy expressions. The nucleation pressure expressions

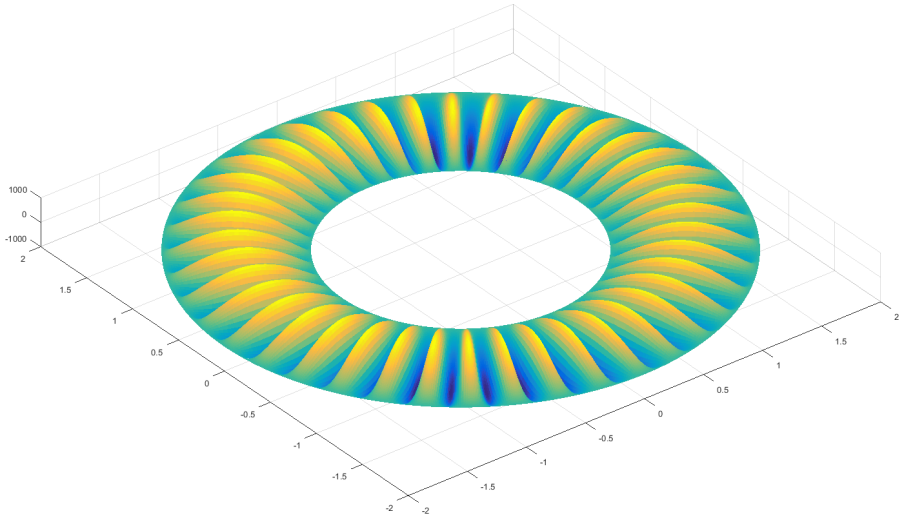

Figure 5: The suggested form of wrinkling which includes a sinusoidal radial dependence. The wrinkling is portrayed in the r-z plane.

are as follows:

$$\Pi_{\text{nuc, simple, strain}} = \frac{\gamma_1 \ln\left(\frac{b}{a}\right)}{\left(\frac{b^2}{b^2-a^2}\right)\ln\left(\frac{b}{a}\right)+\frac{1}{2}} \tag{10}$$

$$\Pi_{\text{nuc, simple, stress}} = \frac{F\gamma_1 \ln\left(\frac{b}{a}\right)}{F\left(\frac{b^2}{b^2-a^2}\right)\ln\left(\frac{b}{a}\right)+\frac{1}{2}} \tag{11}$$

$$\Pi_{\text{nuc, radial, strain}} = \frac{\gamma_1 \int_a^b \frac{\sin^2 R}{r} dr}{\frac{a^2b^2}{a^2-b^2}\int_a^b \frac{\sin^2 R}{r^3} dr + b^2 \int_a^b \frac{\sin^2 R}{r} dr} \tag{12}$$

$$\Pi_{\text{nuc, radial, stress}} = \frac{\gamma_1 F \int_a^b \frac{\sin^2 R}{r} dr}{\frac{a^2b^2}{a^2-b^2}\int_a^b \frac{\sin^2 R}{r^3} dr + b^2 F \int_a^b \frac{\sin^2 R}{r} dr} \tag{13}$$

3 Methods

A thin film of polystyrene is formed on a glass slide and then annuli are cut out of it using sharp tweezers. This is then placed into water which allows the polystyrene to float on water. It is then possible to separate the annulus from the rest coating on the slide by pulling with tweezers. The process of spin coating will be explained in section 3.1. The floated annulus then requires the surface tension to be changed. This process is elaborated upon in section 3.2. The number of resulting wrinkles needs to be determined using image analysis which is explained in section 3.3. The image quality can be improved by using different shapes of scatterers to generate lighting gradients. If these gradients fall across the annulus the resulting image allows for much easier counting of wrinkles and so a short investigation into the best form of lighting was done. The details of this short investigation are contained in section 3.4.

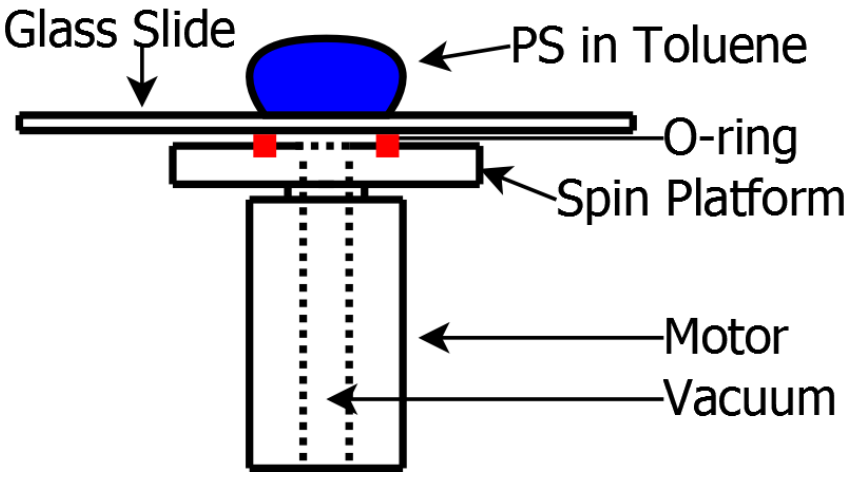

Figure 6: A schematic diagram of the spin coater used to make the polymer films.

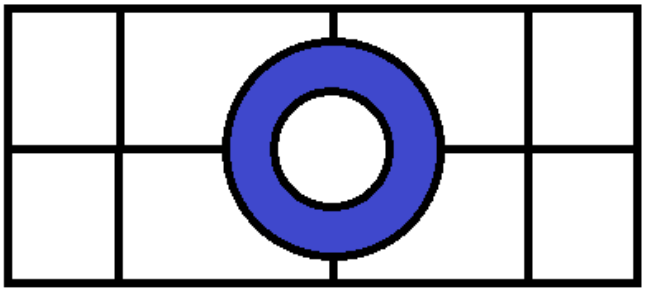

Figure 7: An illustration of the cuts made to the thin film of polystyrene to allow an annulus to be extracted from the plate easily. The annulus is shown in blue and the white sections are polystyrene that is removed after the film is floated.

3.1 Sample Preparation and Thickness Measurement

To make the annuli, a solution of $\sim$ 2% polystyrene was added to toluene and left to fully dissolve. A glass microscope slide was broken in half and placed onto the spin coater which held the slide in place using a vacuum pump as shown in Fig. 6. A few drops of the polystyrene solution were added to the centre of the half slide and then the slide was spun at $\sim$ 2500 rpm or $\sim$ 3000 rpm to generate a thin film of polystyrene. Sharp tweezers were used to cut two concentric circles while the sample spun, making an annulus. The outside of the annulus was then scored to form the pattern shown in Fig. 7. Doing so allows the film to float off the slide more easily by giving the water somewhere to penetrate. The cuts also makes it easier to remove the excess without damaging the annulus.

To measure the thickness, a half slide was coated as before and then the full film was floated onto water. A piece of silicon was brought up from underneath the polystyrene to transfer the thin film to the silicon. This silicon was then placed in a single wavelength (633 nm) self nulling ellipsometer to measure the thickness of the film. This was repeated for any new solution mixed at each speed used. The thicknesses measured in this experiment are included in table 8.

Solution	Spin Rate (rpm)	Thickness (nm)
1	3000	80 ± 2
2	3000	83 ± 7
3	3000	82 ± 2
1	2500	91 ± 5

Figure 8: Table of film thicknesses used in the experiment

3.2 Imaging Wrinkled Annuli

To measure the elastic modulus of a thin film using the maths derived previously, the surface tensions inside and outside of an annulus of the thin film needs to be carefully controlled. This can be done by adding small amounts of surfactant around the annulus and reducing the area the surfactant occupies to decrease the outside surface pressure. A Langmuir-Blodgett (LB) trough is used. LB troughs have movable PTFE barriers which contact the surface of the subphase and allow compression of the surface. The number of wrinkles as a result of a surface pressure difference needs to be determined. To do this, a 4 MPx camera is mounted vertically above the annulus and diffuse lighting is applied vertically through the use of a beam splitter. This allows the bending of the annulus to scatter off the surface and reduce the brightness in points where the normal to the surface is not vertical, thus wrinkles appear lighter or darker than the surrounding material. The set up described is illustrated in Fig. 9.

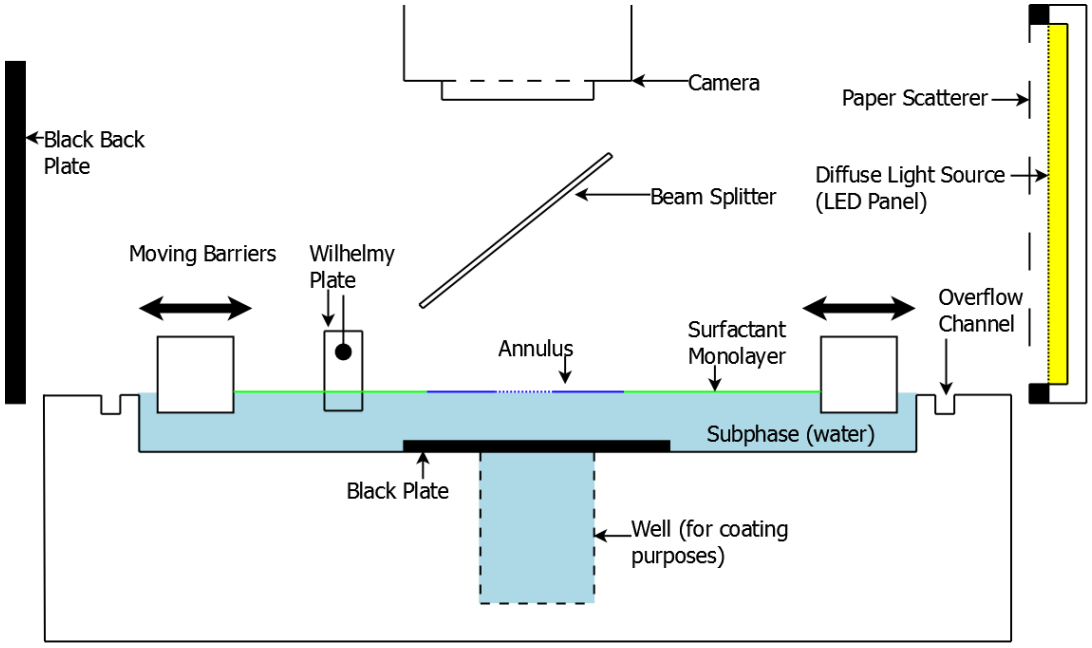

Figure 9: A schematic diagram of experimental arrangement. The barriers are controlled using a computer and the image acquisition is triggered manually. The surface pressure at the time of imaging is saved in the file name of the image. The images are later analysed, automatically counting the number of wrinkles.

The Wilhelmy plate is a rectangle of absorbent paper attached to a sensitive load sensor. The measurement from the device is sent to a ADC interface which allows the force to be determined from current. The Wilhelmy plate can only measure relative surface pressure so the trough must be thoroughly cleaned. Dichloromethane was used as it readily dissolves span-80 and polystyrene. Once the trough is clean, de-ionised, distilled water is used to fill the trough. The surface is then cleaned using a small Bernoulli's principle pump to remove any dust or

residue. A new piece of filter paper is then hung so that is sits partially submerged in the water. The reading on the plate is zeroed so that the reference surface tension is water. To verify that the trough has no residual contaminants, the barriers are fully closed and opened again. If the surface pressure stays constant around zero, then the water is clean. If not, the barriers are closed and the pump is used more, or the water is replaced if the water is very dirty ($\Pi_{\max} > 5$ mN/m).

The scored slide can then be carefully placed into the water, angled downward so that water can separate the slide and polystyrene. The film will then float and the slide will sink. The excess polystyrene can be picked up by touching it with clean tweezers. The inside circle can be removed by picking it out with tweezers. Doing so draws clean water up, setting $gamma_1$ to be that of water. The annulus can be moved by paddling the water in front of the annulus with clean tweezers.

A background image is taken so that the background lighting can be removed from the other images. Then the unwrinkled annulus is imaged so that the sizes of the annulus can be found using an accurate, but slow, algorithm. Drops of surfactant are then added to the outside of the annulus until the surface pressure has increased. The barriers are then moved inwards, taking images after each movement. The size of the steps the barrier takes is controlled manually to adjust for the sensitivity of wrinkles to surface pressure changes. The surface pressure is increased until the annulus crumples under the stresses.

This experiment used dilute span-80 as the surfactant on a water sub-phase. Purified water was used at room temperature (23°C) which has a surface tension of $\gamma_1 = 72.5$ mN/m[18]. Span-80 has a surface tension of $\gamma_{2,min} \approx 38$ mN/m[19] which limits the range of surface tension difference to $\Pi_{max} \approx 40$ mN/m. This limits the maximum size of the annulus to be that of one with $b \approx 12$mm and $a \approx 6$ mm at the thicknesses used. Any larger annulus will not wrinkle sufficiently under the forces applied.

The surface area control is accurate to $A_{\text{acc}} \sim 0.5$ cm^2 with a precision precision of $A_{\text{pre}} \sim 0.1$ cm^2 which allows for surface pressure changes in the order of $\Pi_{\text{pre}} \sim 0.1$ mN/m with an accuracy of $\Pi_{\text{acc}} \sim 0.3$ mN/m.

3.3 Image Processing and Data Analysis

Images are taken of the annulus at various pressures and the aim is to automatically count the number of wrinkles associated with that pressure and to calculate the elastic modulus from the rate of wrinkle growth. The size of the annulus must also be determined from the images. This subsection will describe the various steps taken to achieve this extraction of information required to calculate the elastic modulus. To start, the background is removed and the rough sizes and positions of the annuli are determined for each image. A more accurate size is then found using another method of shape detection, which only works on the unwrinkled annuli, so is done once. A radial intensity profile is taken for each image and peaks and troughs in this profile are identified and counted as the wrinkles. This count is squared and plotted as a function of the surface pressure such that the gradient can be found for the linear region. The conversion from pixels to real size will also be outlined.

The images are saved with the surface pressure at the time of taking stored in the file name. The surface pressure is extracted from them using regular expressions. The first image to be loaded is the background image so this is directly subtracted from all the other images to remove any gradients in lighting on the background plate. This improves contrast. A copy of the images is then converted into a binary (black and white) image using a threshold value. Since the background is removed the threshold can be low. Another copy is made of the binary image

but is inverted. This gives one image where the annulus is white on a black background and one where the annulus is black on a white background. A function called "bwconncomp" is used (Appendix C lines 63-112). Its primary function is to find all groups of white pixels that are connected (touching) and to group them into objects. The resulting objects are in the form the locations of the pixels that make up the objects. The objects are sorted by size so that the anomalous objects are removed. The largest image in the first binary image is the annulus itself and the second largest object in the inverted image is the area that was removed from the middle of the annulus. These objects are illustrated in Fig. 10. The lengths of each of these pixel arrays is equivalent to the area, and so the radii can be determined using

$$A_{\text{outer}} = A_{\text{annulus}} + A_{\text{inner}} = \pi b^2 \tag{14}$$

$$A_{\text{inner}} = \pi a^2 \tag{15}$$

where A represents the areas and a and b are the inner and outer radii respectively. The centres of the circles are found by averaging the x and y positions of all the pixels in the two objects.

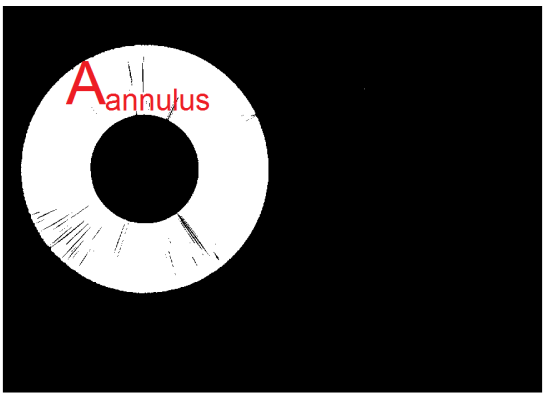

(a) An image of the binary image of a heavily wrinkled annulus. This image is used to find the area of the annulus.

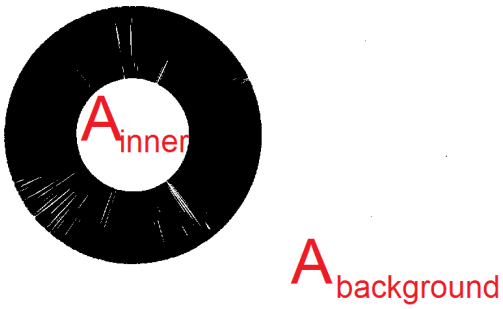

(b) An image of the inverted binary image of a heavily wrinkled annulus. This image is used to find the area of the inner circle removed from the annulus.

Figure 10: Binarised images of a heavily wrinkled annulus with the objects found by "bwconncomp" labelled. These are the objects used to find the centre and radii of the annulus. The annulus is of radii $a = 3.9$ mm and $b = 9.0$ mm subject to a surface pressure of $\Pi = 39.66$ mN/m. 10a shows the thresholded binarised image and 10b shows the inverted thresholded binarised image

To find a better (more accurate and precise) measure of the radii, a and b, the MATLAB function called "imfindcircles" is used (see Appendix C lines 112-135). This function uses Hough transforms (by default) to detect the edges in an image and then determined the size and position of any circles from that Hough transform. This is used on an image of the unwrinkled annulus for highest accuracy and reliability. A 5σ Gaussian blur is applied to the image to improve detection reliability, however, subsequently decreases precision.

To extract intensity profiles, the coordinates of circles of increasing radii are determined such that they cover every pixel in the annulus (see Appendix C lines 154-189). This array of positions is generated for each image. The intensity of each pixel in the image is extracted at each coordinate and is stored in such a way that each row in the resulting array is a circle of certain radius. The circles of smaller radii have reduced angular resolution relative to the outer edges of the annulus. This means that the wrinkle count saturates at around $n = 200$. Because of this, the outside half of the radii circles are considered. The average of these intensity

profiles is taken along the angular direction so that the average intensity along a line directed radially outward is determined. The resulting mean is the intensity profile of the image and the MATLAB function "findpeaks" is used to count the peaks and then used on the negative of the intensity profile to count the troughs. The mean of number of peaks and troughs is used as the resulting count. The inner half of the circle is also counted, for comparison and to determined the extent of the partial wrinkle formation. The "findpeaks" command was given parameters to control the maximum size of the peaks to avoid counting the variation due to scatters and the minimum size was set to avoid the influence of digital noise.

The number of wrinkles is then plotted as a function of the surface pressures. A linear fit is made on the values which exhibit a linear response. A minimum number of wrinkles is used to select these values. The limit varies with data sets and so is adjusted until the fit looks the best. The limit value is stored so that it can be checked or adjusted later. The resulting fit is then plotted on the line and the predicted nucleation point and inner circle counts are also added (see Appendix C lines 194-273) . The resulting plots look like that in Fig. 23; Appendix C contains the collection of the 10 plots for the interested reader.

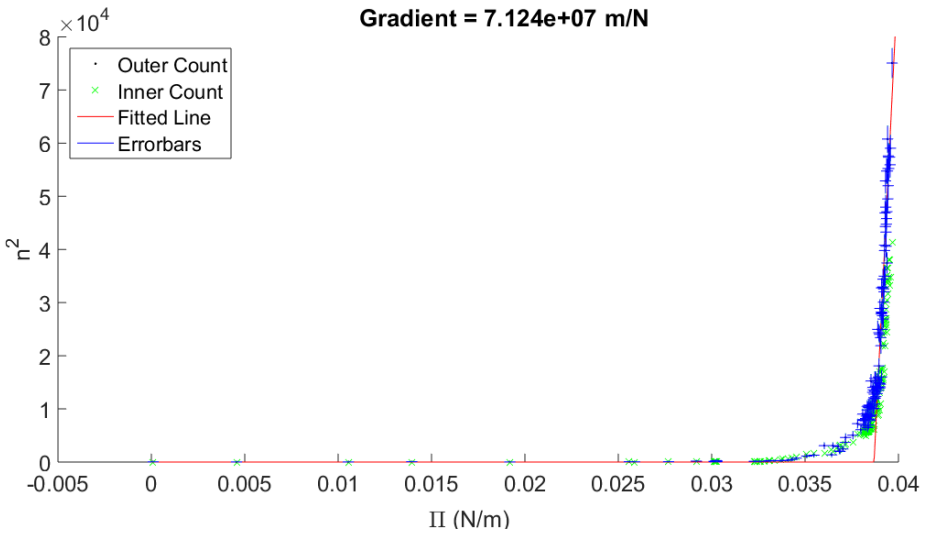

Figure 23: Results for an annulus with $a = 3.8 \pm 0.1$ mm, $b = 7.7 \pm 0.2$ mm and $h = 80 \pm 2$ nm. This gradient produced values for the elastic modulus as $E_{\text{simple,strain}} = 8.25$ GPa; $E_{\text{radial,strain}} = 9.29$ GPa; $E_{\text{simple, strain}} = 16.6$ GPa and $E_{\text{radial, stress}} = 6.63$ GPa (brought forward from page 39).

To extract the real size of the annulus from a size in units of pixels an image of a metal rule was taken and then the MATLAB function "imdistline" was used to determine a length in terms of pixels. This was them simply converted into the real size of one pixel.

3.4 Lighting Investigations

Simply lighting the annulus from above with diffuse lighting was sufficient to image some wrinkles, however the resulting images look flat and lack contrast on the bright peaks in intensity. An example of these flat images is included in Fig. 12. The aim of this section is to describe how it became apparent that it is possible to improve lighting and then the steps taken in order to produce high contrast, three dimensional looking images that drastically improve the peak finding results used in the wrinkle counting process described previously.

When moving a hand in front of the light source to paddle the annulus or adjust the equipment, shadows were cast over the annulus. Any change in gradient from these shadows would greatly

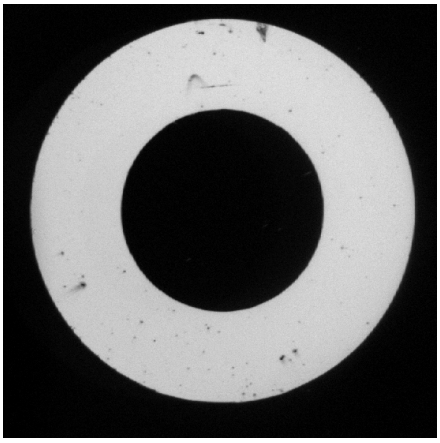

(a) An example image of an unwrinkled annulus under "flat" lighting.

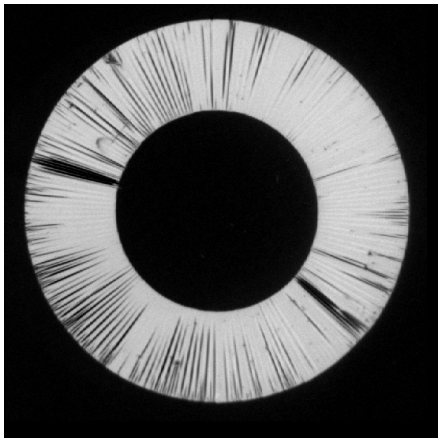

(b) An example image of a wrinkled annulus under "flat" lighting.

Figure 12: Cropped images of an annulus with $a = 4.8$ mm and $b = 9.2$ mm imaged under diffuse light as used by Farmer. The images have low contrast. The background image has been subtracted. 12a shows the unwrinkled image and illustrates the imperfections on the surface. 12b shows the wrinkling at a surface tension difference of $\Pi = 33.2$ mN/m.

increase the contrast on the image, revealing many wrinkles that eluded us. It was clear that it was possible to image the wrinkles much more effectively but the way to do so was less clear. We started an investigation

The first attempt to investigate this was done by simply using fingers over the light source to cast dark shadows onto the annulus. This was fairly effective but cast shadows that were too dark, and so hid wrinkles, and the hand could not be kept still enough. The next step was to use a piece of white printer paper with 25 mm wide slits removed. The paper was clamped over the LED panel so that is cast shadows over the annulus. The bright regions were too wide and so did not show wrinkles near their centres leading to an iterative process of changing the sizes of the bright and dark regions. The best paper scatterer in this example had 19 mm slits separated by 25 mm strips of paper. This formed an image with a gradient in brightness in all regions. An example of the improvements provided by this scatterer is included in Fig. 13. Two aluminium meshes were also tested, however they both lacked large dark regions and so did not provide enough contrast and paper was better.

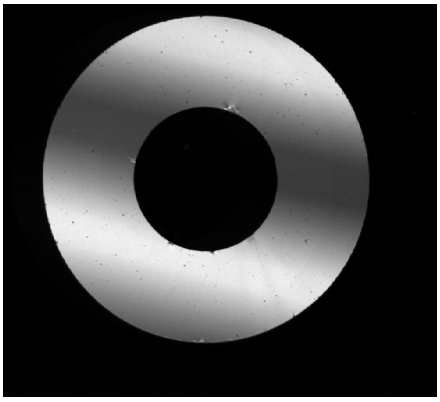

(a) An example image of an unwrinkled annulus under scattered lighting.

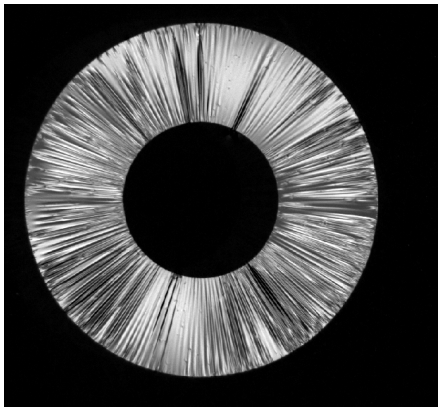

(b) An example image of a wrinkled annulus under scattered lighting.

Figure 13: Cropped images of an annulus with $a = 3.9$ mm and $b = 9.0$ mm imaged under diffuse light with an added scatterer. The images have increased contrast compared to Farmer's method. The background image has been subtracted. 13a shows the unwrinkled image and illustrates the imperfections on the surface. 13b shows the wrinkling at a surface tension difference of $\Pi = 39.9$ mN/m.

4 Results and Analysis

Figure 14 contains all the values for the elastic modulus that were calculated with uncertainties determined by error propagation where possible. It is possible to see that the strain plane models (a and b) produce very similar results, where the addition of a radial buckling term actually increases the elastic modulus: gives a result for a stiffer material. This is not physical since more bending under the same force would represent a less stiff material. In contrast to this, the plane stress models (c and d) follow the expected behaviour: the radial-bending result is much smaller than the angular-only result. This suggests that the mathematics of these models is more physical and therefore justifies its use. The result of the simple stress model is the largest of all the results where the radial stress is the smallest overall.

For all models, the deviation in the elastic modulus values is large and the uncertainties on the values are small therefore the mean, and corresponding error, does not necessarily represent the data. It is clear to see that the results are in such a large spread that the mean does not fit the data well. The deviation is likely to stem from the acquisition of the gradients. The data in Fig. 15 to 23 display obvious inconsistencies in the data collection process. Both the number of images taken and the distribution of pressures changes drastically between figures. Figures 18 to 23 show close fits to the linear section and lots of evenly distributed points compared to the others. These, not coincidentally, produce lower values for the elastic modulus (dataset numbers 5-10) and so it seems easy to conclude that having better datasets can produce smaller values for the elastic modulus.

The expected value of the elastic modulus for polystyrene is[2]

$$E_{\text{polystyrene}} = 3.2 - 3.4 \text{ GPa}$$

where Farmer had a value of

$$E_{\text{Farmer}} = 50 \pm 10\text{GPa}$$

If the results that have the best fits are selected, so only datasets 5-10 are used, a result for the elastic modulus can be calculated as $E_{\text{radial, stress}} = 8 \pm 1\text{GPa}$ which is well within a factor of 3 of the expected result. This suggests that with more data of this quality, or better, the result

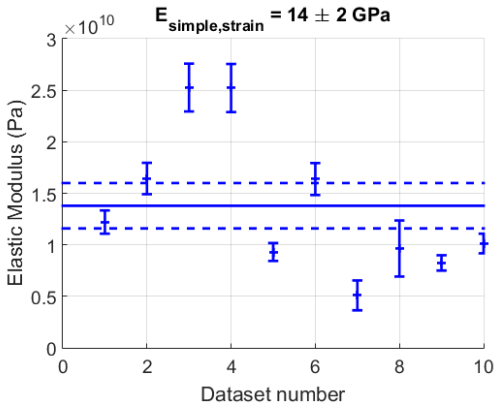

(a) Results for $E_{\text{simple, strain}}$. This is the model originally used by Farmer.

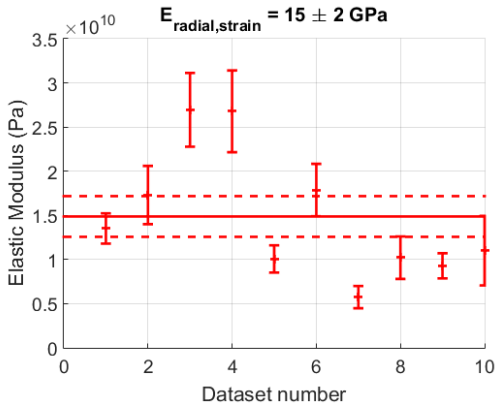

(b) Results for $E_{\text{radial, strain}}$. This is the model used by Farmer but with the addition of a radial bending term.

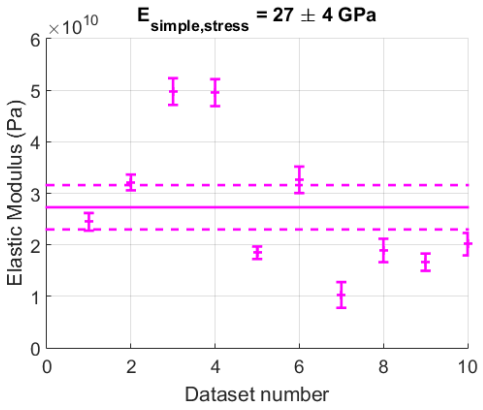

(c) Results for $E_{\text{simple, stress}}$. This is the model using a strain plane to plane stress conversion of the original model. This produces the worst value of the four models.

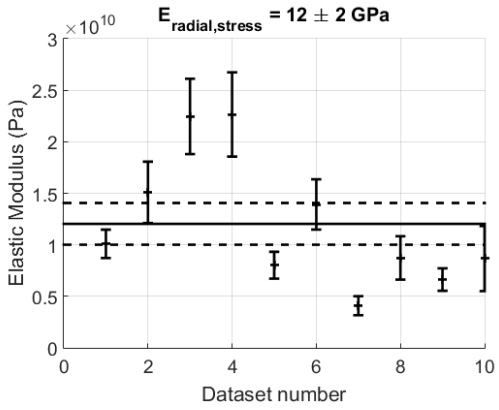

(d) Results for $E_{\text{radial, stress}}$. This is the model which combines the radial term with the plane stress conversion to produce the most physical model of the four models.

Figure 14: Plots of the results for each of the mathematical models described previously. The x-axis is the number assigned to each set of images based on the order they were acquired. This is done for ease of comparison. The solid horizontal line shows the mean and the dashed lines represents the standard error on the mean.

could tend towards the expected value. Since dataset 7 produced a value of $E = 4 \pm 1$GPa and has a reasonable fit, it is possible that the model does actually produce accurate value of the elastic modulus, if the data is good enough.

To verify the models, the nucleation points from each model, after simplifying, was tested for dataset 8. For this dataset, the fitted line intercepts the x-axis at 30.3 mN/m. The four models predicted the nucleation point as

$$\begin{aligned}
\Pi_{\text{nuc, simple, strain}} &= 31.8 \text{ mN/m} \\
\Pi_{\text{nuc, simple, stress}} &= 39.8 \text{ mN/m} \\
\Pi_{\text{nuc, radial, strain}} &= 32.9 \text{ mN/m} \\
\Pi_{\text{nuc, radial, stress}} &= 40.6 \text{ mN/m}
\end{aligned}$$

so all of them are the same order of magnitude and they all sit above the actual nucleation point. This is true for all datasets used in this report. The worst prediction consistently comes from the radial stress model which provides the best result for the elastic modulus but seems

to be the least accurate for this. This raises questions about the validity of the model, however it must be noted that many terms had to be neglected in order to get a result of the right order of magnitude for both radial models.

The attempt to verify the models by using the predicted nucleation points was not successful. Using the full expressions from the appendix (Eq. 70 to 71) determined the radial nucleation pressures to be in the hundreds of N/m range. This is clearly not physical. The cause was narrowed down and so the problematic terms are no longer considered, giving the expressions in Eq. 12 and 13. The neglected terms in the other two expressions are simply negligibly small. Upon further analysis it was found that the largest contributing terms to the nucleation pressures in these models was the constant terms that are not affected by the pressure. If these terms are ignored the results are those displayed above. The simplified expressions are not perfect but they do managed to generate pressures that are producible in the experiment. It is likely that the expression used to find the constants (Eq. 54) is flawed and if the correct model can be derived it may be possible to predict the nucleation and to evaluate the elastic modulus more accurately.

5 Discussion

The aim of the report is to assess the suitability of the experimental techniques for measuring the elastic modulus of thin film materials. To do so, the models derived in this report will be discussed and compared to each other before the sources of error are outlined. Some complications, that arose during the experiments, will be discussed before the methods for error analysis are described.

5.1 Assessing and Comparing the Models

In developing the mathematical models it became apparent that numerical integration was required to determine the values of some terms. This is because the integrands were of the form of sinc functions ($\frac{\sin(x)}{x}$) which cannot be analytically integrated. It also became apparent that the verification of the models would require four conditions to be satisfied. Primarily we require that the wrinkles grow how we expect. Next we require that more bending on a material under the same load yields a smaller elastic modulus value. We also require that the models predict the nucleation pressure somewhat accurately, accounting for various contributions to early nucleation described later. Finally we require that the resulting values of the elastic modulus are of the correct order of magnitude.

All of the models predict that there will be no wrinkles until a nucleation pressure is reached at which point the wrinkles will start to form. The rate of wrinkle growth is predicted to be linear when plotted as n^2 as a function of Π as shown in Fig. 3b. The plots in Fig. 15 to 23 show that the wrinkles do not suddenly start to grow linearly but instead the number of wrinkles bends up toward the linear section. This is thought to be due to the partial wrinkling effects that were observed. It seems likely that the fact that the model assumes that all wrinkles are evenly spread around the annulus and are not thin wrinkles in various locations, that the nucleation behaviour is not physical. It is, however, clear that the wrinkle growth becomes linear at higher pressures, where full wrinkles are most common. In this regime, a linear fit can easily be found and used to determine the observed nucleation point.

The previous attempt, performed by Farmer, failed to account for the buckling of the annulus in a radial direction. We aimed to account for that but found that the result was non-physical: the form with more bending gave a stiffer material. This lead to an investigation into the root of

this problem and it was realised that the mathematics was describing a plane strain problem i.e. one where all the displacements are in plane where the forces act in any direction. The problem we face contains forces only acting in the plane which cause out of plane buckling. This type of problem is a plane stress problem. Slaughter described the similarities between the problems and continued to describe the way to convert the result of one approach into the other[17]. This conversion was done for both models: with wrinkling ignoring the radial buckling and for wrinkling accounting for the radial buckling. The results from this model showed that adding more bending reduced the elastic modulus of the material and therefore seems physical.

The nucleation pressures predicted by our models were never accurate. The biggest problem arose in calculating the nucleation pressure for the radial models. The values of some of the integral terms were several orders of magnitude larger than the surface pressures we achieved. This is a significant problem and lead us to investigate the root of the cause. It was found that all of the terms with numerical integration included were derived from the energy of the form of wrinkling (Eq. 54). This leads us to believe that the value of the energy stored in the internal forces of the annulus, when wrinkled, are not described by the equations used. It is possible that the equation is only valid for plane strain problems and so another one needs to be found (or derived from first principles) for this plane stress problem.

The nucleation pressure prediction equations for the simple models consist of the sum of two terms where the latter is negligible. In an attempt to compare with the radial models, we neglected the terms which correspond to the negligible terms in the simple models such that the result nucleation point expressions become those used. Coincidentally, the negligible terms in the simple models are the same terms that have a higher order of magnitude than expected in the radial models and so this improves the results drastically. There is still a large discrepancy but the results are close enough that, for the sake of this report, the models will still be used.

The nucleation pressures predicted by the models were above the nucleation pressure. This is possibly caused by several different sources of error. It has been observed that the annulus forms partial wrinkles, wrinkles that do not spread across the whole width of the annulus, which allows for energy to be converted into wrinkles which are not counted. These wrinkles disturb the equilibrium position required for the models to hold since they compare the unwrinkled state to the wrinkled state. The models only account for entire wrinkles that are evenly distributed around the annulus. This is suggested to have the largest effect on the nucleation pressure that we observe.

The water used to fill the trough is purified, deionised water and so should have the surface tension that we used for γ_1 however residual contaminants from previous measurements were common. Dichloromethane was used to scrub the trough, however it was still necessary to vacuum contaminants off the surface of the water. The contaminants that were not successfully removed, possibly due to being adsorbed to the Wilhelmy plate or dissolved in the water, may contribute to the discrepancy between the predicted and observed nucleation pressures.

The annuli used in the experiment were of varying quality. Two common problems occurred when spin coating the glass slides, the first was that the edges of the annulus would be torn instead of cut cleanly. The second is that dust and shards of glass remained on the slides. Pure nitrogen was sprayed onto the slides in an attempt to remove the contaminants but this was not always successful. This meant that some annuli formed wakes around the particles during spin coating. Both of these problems lead to premature nucleation because it introduces defects in the annulus. These defects cause weaknesses in the annulus and allow for wrinkles to form more easily.

All of the described effects cause the nucleation to be observed under less pressure than predicted

by the models and therefore it is possible to conclude that the elastic modulus measurements, which are independent of the nucleation pressures, are still valid results.

5.2 Sources of Errors and Uncertainty Estimation

Outside influences contributed to the quality of the results. The sizes of the annuli, the thickness of the annulus, the number of wrinkles and the surface pressure differences all have uncertainty associated with them. The causes of the uncertainty vary and not all causes can be accounted for. For the conversion from pixels to real sizes the uncertainty stems from the rule not being held at the same height as the annulus would be, and that the annuli would not always be at the same height. This causes a small error in the conversion, but primarily the actual number of pixels in three centimetres was counted using a blurred image with resolution that did not create a distinct edge on the markings on the rule. The algorithm used to determine the radii in terms of pixels is also not perfect. A Gaussian blur with standard deviation of five pixels was applied to the images before the algorithm was used. This aided the edge detection but reduced the accuracy of the measurement. All of these errors contribute to the estimate of uncertainty to be a blanket 0.1 mm and 0.2 mm for a and b respectively.

The uncertainty on the thickness of the film is determined in the ellipsometry process. Large uncertainties are caused by the sample film being wrinkled or having pockets of water or air in them. This leads to measurements of the thickness to vary drastically due to the nature of the technique.

The uncertainty on the gradients were taken from the MATLAB "fit" function which provides a 1σ confidence interval estimate on all output variables. It is an underestimate of the uncertainty on the value, since it only considers the linear region. Ideally, instead of a linear fit, a way to fit the data using the predicted growth of wrinkles would be used. An attempt was made to fit the data using the following function:

$$f(\Pi) = \mathrm{Re}(G\sqrt{x - \Pi_{\mathrm{nuc}}})$$

however the fit was worse than using a manual linear fit. This is because the transition between unwrinkled and wrinkled states of the annulus are slowed by the formation of partial wrinkles i.e the line bends up instead of discontinuously changing.

The number of wrinkles is determined through an automated process that searches for peaks and dips in intensity of the expected magnitude of a wrinkle. The tweaking of the upper and lower limits for the prominence of the peaks was necessary and was done until there were no peaks detected on an unwrinkled annulus. The upper limit was set so that the fluctuations in lighting from the scatterer were not considered peaks. The resulting magnitude of the peaks overlies large digital noise from the camera and can cause extra wrinkles to be counted and for some wrinkles to be missed. To check the function of the wrinkle counting process, two partially wrinkles annuli, from different datasets, had their wrinkles manually counted. This count was compared to the count from the automated process. The counts were within 5 wrinkles in 100 for the first and 10 wrinkles in 130 for the other. The uncertainty was set to be a relative measure from this at around 10%.

The surface pressure measurement fluctuates due to digital noise and influences from air currents and liquid disturbances. Since the Wilhelmy plate was not isolated from the air, it was easily disturbed by and movement in air generated by the air conditioning, the extractor fan in the fume hood or people in the laboratory moving near the trough. The air conditioning and the fume hood extractor were turned off during the acquisition of the images, when possible, but the influences from people, and any other sources, were not removed. The combination of

the sources of error lead to a fluctuation on the surface pressure measurement in the order of 0.3mN/m.

5.3 Other Complications

The span-80 surfactant was first diluted in water such that it formed a suspension of colloids. These colloids would be added to the trough alongside the water they're suspended in. Usually the colloids would disperse and form a bilayer film on the surface of the liquid in the trough, reducing the surface tension. Sometimes these colloids would not disperse on contact, even when the liquid was stirred. These colloids would then later disperse, during the image acquisition stage of the experiment, and would often crumple the annuli by suddenly and dramatically increasing the surface pressure. This would render the annulus useless and force the experiment to be restarted.

The trough was filled so that the water would rise just above the edges of the trough such that the surface tension held the water in place. This ensured a good contact with the barriers so that the surfactant would be kept within the desired area. Sometimes the trough would be overfilled such that the reduction is surface tension by the surfactant would overflow the trough, rendering the results useless. This occurred in the acquisition of Fig. 16 but with less devastating consequences. Usually the annulus would float to an edge and get stuck on a part of the trough or it would leave the confines with the overflowing water. In Fig. 16 the data acquisition was continued but it is clear to see that the zero point of the surface pressure was changed significantly.

For all of the models, the forces acting on the edges of the annulus are assumed to be uniform and acting in plane. In reality the surface tension of the water would act differently from the top to the bottom of the edge. For the sake of the model, this was estimated to be uniform because the films used are thin but a more rigorous model would describe the variation of the force at the edges. This is likely to be a source of significant uncertainty, and may reduce the nucleation pressure significantly if the forces act with a vertical component.

The surfactant used, span-80, has a surface tension of $\gamma_{2\ \max} \approx 38\text{mN/m}$[19] which means that the maximum surface pressure that could be produced in this experiment is of the order of 40mN/m. This limits the maximum size of the annulus that can be used. For the thicknesses used in this report, the largest annulus that could be wrinkled had radii around $a = 6$ mm and $b = 11$ mm but for thicker films the maximum size becomes smaller. For thinner films larger annuli could be used. The size of the annulus has an effect on the angular resolution possible for wrinkle counting so either the camera needs to be a higher resolution or a different technique will be required to measure significantly thicker films.

5.4 Error Analysis

The uncertainty on each value of the elastic modulus was calculated using error propagation equations listed in Appendix B. This is straightforward for the simple models however become more complicated for the radial models. The radial models contain integrals which were calculated numerically. It was not possible to determine a way to partially differentiate the integrals to analytically calculate the uncertainty and so to estimate the uncertainty on the integrals, we calculated the integrals using a range of value of a and b according to their corresponding confidence intervals (0.1mm and 0.2mm respectively). The values with the largest difference in each direction were extracted. The mean of these magnitudes were then used as the uncertainty on the integrals. The uncertainties calculated were used in the error propagation equations

where all other variables were considered normally. This method gives a suitable magnitude of uncertainty and so we can justify using it.

The uncertainty on the final values, acquired from and plotted on Fig. 14, were calculated using the standard error on the mean equation which is

$$\delta S = \frac{\sigma}{\sqrt{N}} \tag{16}$$

where δS is the uncertainty on the mean, σ is the standard deviation of the results and N is the number of data points used.

6 Opportunities for Improvement

The uncertainties in this experiment are quite large. Several things can be done to reduce them such as reducing the fluctuation on the surface pressure measurements by isolating the apparatus from air currents and disturbances. The error on surface pressure can be reduced by taking the mean of several measures of the pressure for each image. Alternatively many more images can be taken at the same pressure. To avoid sudden crumpling of annuli, the span-80 can be mixed into the water more thoroughly. To more accurately measure the radii of the annuli, the conversion can be made more accurate by using a better rule or by making the conversion from several measurements.

To improve the mathematical model, it is probably necessary to derive the expressions for the wrinkling energies from first principles and to start again. Ideally the model will describe the nucleation, the wrinkle growth and the forces on the side more accurately than this model does. It may also be possible to verify the form of the bending that is derived. It may be possible to determined the shape of the wrinkles by measuring the intensity of light in different ways or at different angles. This shape can then be compared to the form of the wrinkling derived in the model.

It may be possible to determine the exact shape of the resulting wrinkles by using various optical techniques with the aim to find the shape of various parts of an annulus. If the model can be derived, attempts should be made to confirm that the annulus behaves how the maths predicts. If a higher resolution camera were to be used, it may be possible to measure the change in the radii. This could be used to determined whether the derived form of bending is correct (Eq. 43 and 50). Currently the form of radial compression is assumed to follow this, however no measurements have been made to confirm this. Measuring the changes in a and b as a function of force may allow for the confirmation of the form of compression. As for the profile of the wrinkles, observing scattering from a point source may form the base of a method to determine the shapes on the annulus to verify that it bends with the forms suggested by this model.

Once a new model is derived, it should then be used to measure the elastic properties of films in a large range of thicknesses in an attempt to observe the change in material properties as the film approaches the e-e RMS distance that characterises ultra-thin films. It may then be possible to learn more about free surfaces of polymer structures.

7 Conclusions

The aim of this report was to investigate the possibility of measuring elastic properties of ultra-thin films by using a Langmuir-Blodgett trough to cause capillary wrinkling of a thin film annulus. This was conducted successfully however a mathematical description was not yet

determined to accurately describe the wrinkling. Furthermore the wrinkle count could not be used to produce an acceptable result for the elastic modulus of a relatively thick film. Therefore the conclusion is that the report was not a success, however has generated significant insight into the problem and shows that the behaviour of the annulus is predictable. This gives reason to believe that it is possible to measure elastic properties of a thin film if the model can be derived correctly. There is possibility to improve the data by taking more surface pressure measurements for each number of wrinkles and by reducing the effect of airflow on the surface pressure measurements.

The report simultaneously aimed to corroborate Farmer's conclusion that it could be possible if the mathematical problems could be overcome and to improve the results acquired by using his technique. We have achieved much more accurate results and with higher precision. The expected bulk value of elastic modulus for polystyrene is $E_{\text{polystyrene}} = 3.2 - 3.4\text{GPa}$ where we managed to reduce Farmer's result from $E_{\text{Farmer}} = 50 \pm 10\text{GPa}$ to $E_{\text{radial, stress}} = 12 \pm 2\text{GPa}$, by deriving a model to describe another form of bending and using the expressions for a plane stress problem. The derived problem does not accurately predict the nucleation point of wrinkles and therefore cannot be said to represent the physics properly. The cause of this discrepancy has been isolated but a correction has not yet been implemented.

Overall it can be concluded that the experiment failed to produce a good value of the elastic modulus of a thin film, however great improvements have been made to the previous attempt at doing so. An elastic modulus was measured within a factor of 4 of the expected value. With further work, it seems very likely that elastic properties of films can be determined using capillary wrinkling of annuli. Primarily the mathematical model needs to be derived and verified and secondarily, the surface pressure measurement needs some improvements.

References

[1] D. J. Farmer, *Elastic measurements in ultra-thin polymer structures*. PhD thesis, University of Nottingham, 2016.

[2] J. Brandrup, E. H. Immergut, E. A. Grulke, A. Abe, and D. R. Bloch, *Polymer handbook*, vol. 7. Wiley New York etc, 1989.

[3] L. MatWeb, "Matweb—material property data," *línea]. Available: http://www. matweb. com/search/DataSheet. aspx*, 2013.

[4] A. Voevodin and J. Zabinski, "Supertough wear-resistant coatings with 'chameleon'surface adaptation," *Thin Solid Films*, vol. 370, no. 1, pp. 223–231, 2000.

[5] D. Lee, M. F. Rubner, and R. E. Cohen, "All-nanoparticle thin-film coatings," *Nano letters*, vol. 6, no. 10, pp. 2305–2312, 2006.

[6] J. Sharp and J. Forrest, "Free surfaces cause reductions in the glass transition temperature of thin polystyrene films," *Physical review letters*, vol. 91, no. 23, p. 235701, 2003.

[7] R. Dingreville, J. Qu, and M. Cherkaoui, "Surface free energy and its effect on the elastic behavior of nano-sized particles, wires and films," *Journal of the Mechanics and Physics of Solids*, vol. 53, no. 8, pp. 1827–1854, 2005.

[8] Merriam-Webster, *Merriam-Webster's collegiate dictionary*. Merriam-Webster, 2004.

[9] M. P. Stevens, *Polymer chemistry: an introduction*. oxford university press New York, 1999.

[10] I. Teraoka, *Polymer Solutions: An Introduction to Physical Properties*. John Wiley and Sons, Inc, 2002.

[11] R. A. Jones, *Soft condensed matter*, vol. 6. Oxford University Press, 2002.

[12] D. F. Evans and H. Wennerström, "The colloidal domain: where physics," *Chemistry, Biology, and Technology Meet*, vol. 2, pp. 193–197, 1999.

[13] M. Geoghegan and G. Krausch, "Wetting at polymer surfaces and interfaces," *Progress in Polymer Science*, vol. 28, no. 2, pp. 261–302, 2003.

[14] E. Hecht, "Hecht optics," *Addison Wesley*, vol. 997, pp. 213–214, 1998.

[15] H. Tompkins and E. A. Irene, *Handbook of ellipsometry*. William Andrew, 2005.

[16] J. Woollam and A. Inc, "A short course in ellipsometry," *Revised January*, vol. 1, 2001.

[17] W. S. Slaughter, "Two dimensional problems," in *The Linearized Theory of Elasticity*, pp. 387–429, Springer, 2002.

[18] G. W. C. Kaye and T. H. Laby, *Tables of physical and chemical constants: and some mathematical functions*. Longmans, Green and Company, 1921.

[19] L. J. Peltonen and J. Yliruusi, "Surface pressure, hysteresis, interfacial tension, and cmc of four sorbitan monoesters at water–air, water–hexane, and hexane–air interfaces," *Journal of colloid and interface science*, vol. 227, no. 1, pp. 1–6, 2000.

[20] T. Wierzbicki, "2.081 j/16.230 j plates and shells, spring 2006," 2006.

[21] P. Kelly, "Strain energy in plates," in *Solid Mechanics Part II*, p. 182, `http://homepages.engineering.auckland.ac.nz/~pkel015/SolidMechanicsBooks/Part_II/06_PlateTheory/06_PlateTheory_09_StrainEnergy.pdf`, 2013.

A Full Derivation of Elastic Modulus Expression

Given the arrangement described by Fig. 2 it is possible to describe the stresses applied and to determine the strains that are results of these stresses. The stresses and strains will lead to some displacements. It is possible to determine the energy before and after this deformation by considering the strain stored in the bent annulus and the work done by the forces to cause that deformation. This appendix entry will describe the entire process and will result in expression for the elastic modulus as a function of rate of growth of the number of wrinkles with respect to surface pressure changes. First, the approach taken previously by Farmer, which is to consider plane strain, will be attempted for two different forms of wrinkling. Next the approach will be applied to a plane stress situation, which is what is observed experimentally, for both shapes of wrinkling. Finally the energies for the bending and works done will be expressed. From these the elastic modulus will be calculated using the gradient $\frac{dn^2}{d\Pi}$ where n in the number of wrinkles and Π is the surface pressure difference, $\Pi = \sigma_1 - \sigma_2$.

A.1 Plane Strain Approach

The pressures σ_1 and σ_2 generate stresses described by the traction vector $\underline{\hat{t}} = \sigma_{rr}\underline{\hat{n}}$ and so the form of the wrinkling in r can be found and used to find an expression for the energy. The energy minimum as a function of pressure and number of wrinkles will then be found and used to express the elastic modulus as a function of the number of wrinkles. If a force changes the shape of the material, some work is done to change the shape which is equal to the energy stored in the shape a s a result of the bending. The energy stored can be found using the theory of elasticity, which states that under elastic deformation, the stresses and strains in the material can be described in terms of the forces and the properties of the material. In this experiment the elastic modulus and the Poisson ratio are considered. The elastic modulus is a measure of the ratio of one dimensional displacement along the direction of pressure to the pressure applied (how much the material extends or compresses under force). The Poisson ratio is the ratio of tangential displacement under pressure to the normal direction of the pressure (how much the material thins under expansion or widens under compression).

An approach to these problems consists of expressing the stresses in terms of the Lamé coefficients μ and λ using the Lamé-Navier equations $\underline{\sigma} = 2\mu\underline{\epsilon} + \lambda(\text{tr } \underline{\epsilon})\underline{I}$[17] to describe the relationship between stresses applied (σ and the resulting deformations, described by strains (ϵ). The Lamé-Navier equations are the three dimensional equivalent of Hooke's law. The equations in cylindrical polar coordinates take the forms

$$\sigma_{rr} = 2\mu\epsilon_{rr} + \lambda(\epsilon_{rr} + \epsilon_{\theta\theta}) \tag{17}$$

$$\sigma_{\theta\theta} = 2\mu\epsilon_{\theta\theta} + \lambda(\epsilon_{rr} + \epsilon_{\theta\theta} \tag{18}$$

$$\sigma_{r\theta} = 2\mu\epsilon_{r\theta} \tag{19}$$

when expanded. The conversion to write the Lamé coefficients in terms of E and ν are given by the following relations:

$$\mu = \frac{E}{2(1+\nu)} \tag{20}$$

$$\lambda = \frac{E\nu}{(1+\nu)(1-2\nu)} \tag{21}$$

The displacement field (the magnitude and direction of displacement a point moves from its resting position when under load) is assumed to take the form

$$\underline{u} = u\underline{\hat{r}} + v\underline{\hat{\theta}} + w\underline{\hat{z}} \tag{22}$$

where

$$u = u(r) \tag{23}$$
$$v = 0 \tag{24}$$
$$w = w(r, \theta) \tag{25}$$

and only w is considered in the energetic expressions due to it being much larger than u. These can be used to find expressions for the strains in terms of the displacement[17]:

$$\epsilon_{rr} = \frac{\partial u}{\partial r} \tag{26}$$
$$\epsilon_{\theta\theta} = \frac{1}{r}\left(\frac{\partial u}{\partial \theta} + u\right) \tag{27}$$
$$\epsilon_{r\theta} = \frac{1}{2}\left(\frac{1}{r}\frac{\partial u}{\partial \theta} + \frac{\partial u}{\partial r} - \frac{v}{r}\right) \tag{28}$$

By substituting Eq. 23 into Eq. 17 to 19 the strains reduce to

$$\epsilon_{rr} = \frac{\partial u}{\partial r} \tag{29}$$
$$\epsilon_{\theta\theta} = \frac{u}{r} \tag{30}$$
$$\epsilon_{r\theta} = 0 \tag{31}$$

and give us the components of stress given by

$$\sigma_{rr} = (2\mu + \lambda)\frac{\partial u}{\partial r} - \lambda\frac{u}{r} \tag{32}$$
$$\sigma_{\theta\theta} = (2\mu + \lambda)\frac{\partial u}{\partial r} + \lambda\frac{u}{r} \tag{33}$$
$$\sigma_{r\theta} = 0 \tag{34}$$

The next step is to find the form of the radial buckling which can be done by considering the strain field and the equilibrium equations given by Slaughter[17] as

$$\frac{\partial \sigma_{rr}}{\partial r} + \frac{1}{r}\frac{\sigma_{r\theta}}{\partial \theta} + \frac{1}{r}(\sigma rr - \sigma\theta\theta) = 0 \tag{35}$$
$$\frac{\partial \sigma_{r\theta}}{\partial r} + \frac{1}{r}\frac{\partial \sigma_{\theta\theta}}{\partial \theta} + \frac{2}{r}\sigma_{r\theta} = 0 \tag{36}$$

for which the left hand side of the latter is trivially zero and the prior results in a Euler Cauchy equation. The exact form is given by

$$r^2\frac{\partial^2 u}{\partial r^2} + r\frac{\partial u}{\partial r} - u = 0 \tag{37}$$

and has a known solution. The solution to this form of Euler Cauchy has the general form

$$u(r) = Br + \frac{C}{r} \tag{38}$$

where B and C are constants to be determined from boundary conditions.

Because the force only acts at the edges of the plane of the annulus, the boundary conditions define the stress at the edges to be total force at the edge i.e.

$$\sigma_{rr}(r = b) = \sigma_1 \tag{39}$$
$$\sigma_{rr}(r = a) = \sigma_2 \tag{40}$$

and so by substituting this into Eq. 32 we find that

$$B = \frac{1}{2(\mu+\lambda)}\left(\frac{a^2\sigma_1 - b^2\sigma_2}{a^2-b^2}\right) \tag{41}$$

$$C = \frac{a^2b^2}{2\mu}\left(\frac{\sigma_1-\sigma_2}{a^2-b^2}\right) \tag{42}$$

giving, in full,

$$u_{\text{strain}}(r) = \frac{r}{2(\mu+\lambda)}\left(\frac{a^2\sigma_1 - b^2\sigma_2}{a^2-b^2}\right) + \frac{a^2b^2}{2\mu r}\left(\frac{\sigma_1-\sigma_2}{a^2-b^2}\right) \tag{43}$$

and form of u has been found. Now it is possible to fully express σ_{rr} and $\sigma_{\theta\theta}$ using Eq. 17, 18 and 43:

$$\sigma_{rr,\text{strain}} = \left(\frac{a^2\sigma_1 - b^2\sigma_2}{a^2-b^2}\right) - \frac{a^2b^2}{r^2}\left(\frac{\sigma_1-\sigma_2}{a^2-b^2}\right) \tag{44}$$

$$\sigma_{\theta\theta,\text{strain}} = \left(\frac{a^2\sigma_1 - b^2\sigma_2}{a^2-b^2}\right) + \frac{a^2b^2}{r^2}\left(\frac{\sigma_1-\sigma_2}{a^2-b^2}\right) \tag{45}$$

The stress, strain and displacement field equations are now solved for the plane strain problem.

A.2 Plane Stress Approach

The observed wrinkling is the result of an in plane stress causing an out of plane displacement. This is the definition of a plane stress problem. To convert the previous expressions from a plane stress equation in to a plane strain equation, expressions relating E, ν, μ and λ to their corresponding plane stress counterparts are required. Thankfully, these are readily available expressions[17]. They are as follows:

$$\mu \to \mu \tag{46}$$

$$\lambda \to \frac{2\mu\lambda}{2\mu+\lambda} \tag{47}$$

$$E \to \frac{E(1+2\nu)}{(1+\nu)^2} \tag{48}$$

$$\nu \to \frac{\nu}{1+\nu} \tag{49}$$

Making the required substitutions in Eq. 43 the radial displacement field becomes

$$u_{\text{stress}}(r) = \frac{r}{2}\left(\frac{a^2\sigma_1 - b^2\sigma_2}{a^2-b^2}\right)\left[\mu + \frac{2\mu\lambda}{2\mu+\lambda}\right]^{-1} + \frac{a^2b^2}{2\mu r}\left(\frac{\sigma_1-\sigma_2}{a^2-b^2}\right) \tag{50}$$

Now, working through as before, using the form of the strains given by Eq. 26-28, our results for the stress field components are

$$\sigma_{rr,\text{stress}} = \left(\frac{a^2\sigma_1 - b^2\sigma_2}{(\mu+\lambda)(a^2-b^2)}\right)\left(\mu + \frac{2\mu\lambda}{2\mu+\lambda}\right) - \frac{a^2b^2}{r^2}\left(\frac{\sigma_1-\sigma_2}{a^2-b^2}\right) \tag{51}$$

$$\sigma_{\theta\theta,\text{stress}} = \left(\frac{a^2\sigma_1 - b^2\sigma_2}{(\mu+\lambda)(a^2-b^2)}\right)\left(\mu + \frac{2\mu\lambda}{2\mu+\lambda}\right) + \frac{a^2b^2}{r^2}\left(\frac{\sigma_1-\sigma_2}{a^2-b^2}\right) \tag{52}$$

and so the displacement, stress and strain fields for the plane stress problem have been solved.

A.3 Energetics

Given the same annulus as previously considered, if the applied stress is enough to deform the annulus it is possible to consider it as an elastic deformation of a plate. Expressions can be found to express the energy stored in the annulus once it has been deformed and to express the work done in bending the plate to that position. The total energy is the difference between these such that $U_{total} = U_{membane} - U_{work}$ The equations for this situation are part of the Theory of Elasticity and so are available in the literature. It is possible to derive the form of the wrinkling, w, however it s far from trivial. To reduce the difficulty of the problem we will use two proposed forms of wrinkling, the first consists only of an angular term, and the second consists of the product of an angular term and a radial terms. Specifically they are given by

$$w_{\text{simple}} = w_o \cos(n\theta) \tag{4}$$

$$w_{\text{radial}} = w_o \cos(n\theta) \sin\left(\frac{\pi(r-a)}{(b-a)}\right) \tag{7}$$

where w_0 is the amplitude of the waves. The shape described by these expressions are shown in Fig. 4 and 5 respectively. The form including a radial term allows for more bending to occur under the same force and should reduce the measured value of the elastic modulus.

The work done by the stresses is found by integrating the stresses over the field given the resultant displacement field, w:

$$U_{\text{work}} = -\frac{h}{2}\int_0^{2\pi}\int_a^b \left\{ \sigma_{rr}\left(\frac{\partial w}{\partial r}\right)^2 + \sigma_{\theta\theta}\left(\frac{1}{r}\frac{\partial w}{\partial \theta}\right)^2 \right\} r dr d\theta \tag{53}$$

and the energy stored in the annulus under stress is found by integrating all the strain components through the volume of the annulus, and can be referred to as the membrane energy[20, 21]:

$$\begin{aligned} U_{\text{membrane}} = \int_0^{2\pi}\int_a^b \Bigg\{ & \frac{D}{2}\left(\frac{\partial^2 w}{\partial r^2} + \frac{1}{r}\frac{\partial w}{\partial r} + \frac{1}{r^2}\frac{\partial^2 w}{\partial \theta^2}\right)^2 \ldots \\ & - D(1-\nu)\frac{\partial^2 w}{\partial r^2}\left(\frac{1}{r}\frac{\partial w}{\partial r} + \frac{1}{r^2}\frac{\partial^2 w}{\partial \theta^2}\right) \ldots \\ & + D(1-\nu)\left(\frac{1}{r}\frac{\partial^2 w}{\partial r \partial \theta} + \frac{1}{r^2}\frac{\partial w}{\partial \theta}\right)^2 \Bigg\} r dr d\theta \end{aligned} \tag{54}$$

where D is a compact constant and takes a different form for plane stress and plane strain. These forms are:

$$D_{\text{strain}} = \frac{Eh^3}{12(1-\nu^2)} \tag{55}$$

$$D_{\text{stress}} = \frac{E(1+2\nu)h^3}{12(1+\nu)^2}\left[1 - \left(\frac{\nu}{1+\nu}\right)^2\right]^{-1} = \frac{Eh^3}{12} \tag{56}$$

where the latter is converted from the prior using Eq. 46-49. It is now possible to determine the energetics of the system given the form of wrinkling w. Two forms of wrinkling were considered, and they will be dealt with separately. First a simplified form of wrinkling was suggested, which had no radial dependence on amplitude as described by Eq. 4 and the second was radially dependent and is given in Eq. 7.

For the simplified form, the total energies take the forms

$$U_{\text{simple, strain}} = \frac{\pi h n^2 w_0^2}{2(a^2-b^2)}\left\{(a^2\sigma_1 - b^2\sigma_2)\ln\left(\frac{b}{a}\right) + \frac{(b^2-a^2)(\sigma_1-\sigma_2)}{2}\right\}... \\ + \frac{\pi n^2 w_0^2 D_{\text{strain}}}{4}\left(\frac{b^2-a^2}{a^2b^2}\right)(n^2+1-\nu) \quad (57)$$

$$U_{\text{simple, stress}} = \frac{\pi h n^2 w_0^2}{2(a^2-b^2)}\left\{F(a^2\sigma_1 - b^2\sigma_2)\ln\left(\frac{b}{a}\right) + \frac{(b^2-a^2)(\sigma_1-\sigma_2)}{2}\right\} \\ + \frac{\pi n^2 w_0^2 D_{\text{stress}}}{4}\left(\frac{b^2-a^2}{a^2b^2}\right)(n^2+1-\nu) \quad (58)$$

for the radially independent form of buckling, where F is given by:

$$F = \frac{2\nu}{1-2\nu} + \frac{2}{\frac{\nu}{1-2\nu}+1} - \frac{1}{\frac{\nu}{1-2\nu}+\frac{1}{2}} \quad (3)$$

For the radially dependent form of buckling they are

$$U_{\text{radial, strain}} = \frac{hn^2w_0^2\pi}{2}\left\{\frac{a^2b^2(\sigma_1-\sigma_2)}{a^2-b^2}\int_a^b \frac{\sin^2 R}{r^3}dr + \frac{a^2\sigma_1 - b^2\sigma_2}{a^2-b^2}\int_a^b \frac{\sin^2 R}{r}dr\right\}... \\ w_0^2 D_{\text{strain}}\left\{\frac{2n^2\pi^3}{(b-a)^2}\int_a^b \frac{\sin^2 R}{r}dr - \frac{2n^2\pi^2}{b-a}\int_a^b \frac{sinR\ cosR}{r^2}dr\ ... \right. \\ + \frac{n^4\pi}{2}\int_a^b \frac{\sin^2 R}{r^3}dr - \frac{n^2\pi^3(1-\nu)}{(b-a)^2}\int_a^b \frac{\sin^2 R}{r}dr + \frac{n^2\pi^3(1-\nu)}{(b-a)^2}\int_a^b \frac{\cos^2 R}{r^2}dr... \\ \left. + n^2(1-\nu)\int_a^b \frac{\sin^2 R}{r^3}dr + \frac{2n^2\pi^2(1-\nu)}{b-a}\int_a^b \frac{sinR\ cosR}{r^2}dr\right\} \quad (59)$$

$$U_{\text{radial, stress}} = \frac{hn^2w_0^2\pi}{2}\left\{\frac{a^2b^2(\sigma_1-\sigma_2)}{a^2-b^2}\int_a^b \frac{\sin^2 R}{r^3}dr + F\frac{a^2\sigma_1 - b^2\sigma_2}{a^2-b^2}\int_a^b \frac{\sin^2 R}{r}dr\right\}... \\ + w_0^2 D_{\text{stress}}\left\{\frac{2n^2\pi^3}{(b-a)^2}\int_a^b \frac{\sin^2 R}{r}dr - \frac{2n^2\pi^2}{b-a}\int_a^b \frac{sinR\ cosR}{r^2}dr\ ... \right. \\ + \frac{n^4\pi}{2}\int_a^b \frac{\sin^2 R}{r^3}dr - \frac{n^2\pi^3\left(1-\frac{\nu}{1+\nu}\right)}{(b-a)^2}\int_a^b \frac{\sin^2 R}{r}dr + \frac{n^2\pi^3\left(1-\frac{\nu}{1+\nu}\right)}{(b-a)^2}\int_a^b \frac{\cos^2 R}{r^2}dr... \\ \left. + n^2\left(1-\frac{\nu}{1+\nu}\right)\int_a^b \frac{\sin^2 R}{r^3}dr + \frac{2n^2\pi^2\left(1-\frac{\nu}{1+\nu}\right)}{b-a}\int_a^b \frac{sinR\ cosR}{r^2}dr\right\} \quad (60)$$

where R is shorthand for the argument of the radially dependant sin term:

$$R \equiv \frac{\pi(r-a)}{b-a} \quad (61)$$

It is now possible to minimise the total energies in terms of number of wrinkles for a given pressure. To do this, the energy is differentiated with respect to n and the minimum is found as the number of wrinkles at which this is zero:

$$\frac{dU_{\text{simple, strain}}}{dn} = \pi n^3 w_0^2 D_{\text{strain}}\left(\frac{b^2-a^2}{a^2b^2}\right) + \frac{\pi n w_0^2 D_{\text{strain}}}{2}\left(\frac{b^2-a^2}{a^2b^2}\right)(1-\nu)... \\ + \frac{\pi h n w_0^2}{(a^2-b^2)}\left\{(a^2\sigma_1 - b^2\sigma_2)\ln\left(\frac{b}{a}\right) + \frac{(b^2-a^2)(\sigma_1-\sigma_2)}{2}\right\} = 0 \quad (62)$$

$$\frac{dU_{\text{simple, stress}}}{dn} = \pi n^3 w_0^2 D_{\text{stress}} \left(\frac{b^2-a^2}{a^2b^2}\right) + \frac{\pi n w_0^2 D_{\text{stress}}}{2}\left(\frac{b^2-a^2}{a^2b^2}\right)\left(1-\frac{\nu}{1+\nu}\right)... + \frac{\pi h n w_0^2}{(a^2-b^2)}\left\{F(a^2\sigma_1 - b^2\sigma_2)\ln\left(\frac{b}{a}\right) + \frac{(b^2-a^2)(\sigma_1-\sigma_2)}{2}\right\} = 0 \quad (63)$$

$$\frac{dU_{\text{radial, strain}}}{dn} = hnw_0^2\pi\left\{\frac{a^2b^2(\sigma_1-\sigma_2)}{a^2-b^2}\int_a^b \frac{\sin^2 R}{r^3}dr + \frac{a^2\sigma_1 - b^2\sigma_2}{a^2-b^2}\int_a^b \frac{\sin^2 R}{r}dr\right\}... 2w_0^2 D_{\text{strain}}\left\{\frac{2n\pi^3}{(b-a)^2}\int_a^b \frac{\sin^2 R}{r}dr - \frac{2n\pi^2}{b-a}\int_a^b \frac{sinR\ cosR}{r^2}dr\ ... + n^3\pi\int_a^b \frac{\sin^2 R}{r^3}dr - \frac{n\pi^3(1-\nu)}{(b-a)^2}\int_a^b \frac{\sin^2 R}{r}dr + \frac{n\pi^3(1-\nu)}{(b-a)^2}\int_a^b \frac{\cos^2 R}{r^2}dr... + n(1-\nu)\int_a^b \frac{\sin^2 R}{r^3}dr + \frac{2n\pi^2(1-\nu)}{b-a}\int_a^b \frac{sinR\ cosR}{r^2}dr\right\} = 0 \quad (64)$$

$$\frac{dU_{\text{radial, stress}}}{dn} = hnw_0^2\pi\left\{\frac{a^2b^2(\sigma_1-\sigma_2)}{a^2-b^2}\int_a^b \frac{\sin^2 R}{r^3}dr + F\frac{a^2\sigma_1 - b^2\sigma_2}{a^2-b^2}\int_a^b \frac{\sin^2 R}{r}dr\right\}... + 2w_0^2 D_{\text{stress}}\left\{\frac{2n\pi^3}{(b-a)^2}\int_a^b \frac{\sin^2 R}{r}dr - \frac{2n\pi^2}{b-a}\int_a^b \frac{sinR\ cosR}{r^2}dr\ ... + n^3\pi\int_a^b \frac{\sin^2 R}{r^3}dr - \frac{n\pi^3\left(1-\frac{\nu}{1+\nu}\right)}{(b-a)^2}\int_a^b \frac{\sin^2 R}{r}dr + \frac{n\pi^3\left(1-\frac{\nu}{1+\nu}\right)}{(b-a)^2}\int_a^b \frac{\cos^2 R}{r^2}dr... + n\left(1-\frac{\nu}{1+\nu}\right)\int_a^b \frac{\sin^2 R}{r^3}dr + \frac{2n\pi^2\left(1-\frac{\nu}{1+\nu}\right)}{b-a}\int_a^b \frac{sinR\ cosR}{r^2}dr\right\} = 0 \quad (65)$$

All of these expressions have two solutions for n, one is trivially when there are zero wrinkles and the other is when the number of wrinkles is finite and in terms of n^2. It is now time to make the substitutions required to express the number of wrinkles in terms of Π. To do so we rearrange Eq. 2 and find the following expressions:

$$\sigma_1 - \sigma_2 = \frac{\Pi}{h} \quad (66)$$

$$a^2\sigma_1 - b^2\sigma_2 = \frac{(a^2-b^2)\gamma_1 + b^2\Pi}{h} \quad (67)$$

Plotting n as a function of Π for these each of these minima gives a plot with the form shown in Fig. 3a. This a square root dependence and so the plot of n^2 as a function of Π gives a linear line as shown in 3b. The point at which the result for n becomes real and n^2 becomes positive is the same point. This will be described as the nucleation point. The nucleation point is the pressure at which the force is sufficient enough to start wrinkling the annulus. This point can be predicted and compared to the real result. The expressions for the nucleation points for each model are found by setting $n^2(\Pi_{\text{nuc}}) = 0$:

$$\Pi_{\text{nuc, simple, strain}} = \frac{\gamma_1 \ln\left(\frac{b}{a}\right) + \frac{D_{\text{strain}}}{2}\left(\frac{b^2-a^2}{a^2b^2}\right)(1-\nu)}{\left(\frac{b^2}{b^2-a^2}\right)\ln\left(\frac{b}{a}\right) + \frac{1}{2}} \quad (68)$$

$$\Pi_{\text{nuc, simple, stress}} = \frac{F\gamma_1 \ln\left(\frac{b}{a}\right) + \frac{D_{\text{stress}}}{2}\left(\frac{b^2-a^2}{a^2b^2}\right)(1-\frac{\nu}{1+\nu})}{F\left(\frac{b^2}{b^2-a^2}\right)\ln\left(\frac{b}{a}\right) + \frac{1}{2}} \quad (69)$$

$$\Pi_{\text{nuc, radial, strain}} = \frac{2D_{\text{strain}}}{\frac{a^2b^2}{a^2-b^2}\int_a^b \frac{\sin^2 R}{r^3}dr + b^2\int_a^b \frac{\sin^2 R}{r}dr}\left\{\frac{2n\pi^2}{(b-a)^2}\int_a^b \frac{\sin^2 R}{r}dr... \right.$$
$$- \frac{2\pi}{b-a}\int_a^b \frac{sinR\ cosR}{r^2}dr - \frac{\pi^2(1-\nu)}{(b-a)^2}\int_a^b \frac{\sin^2 R}{r}dr + \frac{\pi^3(1-\nu)}{(b-a)^2}\int_a^b \frac{\cos^2 R}{r^2}dr...$$
$$\left. + (1-\nu)\int_a^b \frac{\sin^2 R}{r^3}dr + \frac{2n\pi(1-\nu)}{b-a}\int_a^b \frac{sinR\ cosR}{r^2}dr\right\} + \frac{\gamma_1\int_a^b \frac{\sin^2 R}{r}dr}{\frac{a^2b^2}{a^2-b^2}\int_a^b \frac{\sin^2 R}{r^3}dr + b^2\int_a^b \frac{\sin^2 R}{r}dr} \tag{70}$$

$$\Pi_{\text{nuc, radial, stress}} = \frac{2D_{\text{strain}}}{\frac{a^2b^2}{a^2-b^2}\int_a^b \frac{\sin^2 R}{r^3}dr + b^2F\int_a^b \frac{\sin^2 R}{r}dr}\left\{\frac{2n\pi^2}{(b-a)^2}\int_a^b \frac{\sin^2 R}{r}dr... \right.$$
$$- \frac{2\pi}{b-a}\int_a^b \frac{sinR\ cosR}{r^2}dr - \frac{\pi^2(1-\nu)}{(b-a)^2}\int_a^b \frac{\sin^2 R}{r}dr + \frac{\pi^3(1-\nu)}{(b-a)^2}\int_a^b \frac{\cos^2 R}{r^2}dr...$$
$$\left. + (1-\nu)\int_a^b \frac{\sin^2 R}{r^3}dr + \frac{2n\pi(1-\nu)}{b-a}\int_a^b \frac{sinR\ cosR}{r^2}dr\right\} + \frac{\gamma_1 F\int_a^b \frac{\sin^2 R}{r}dr}{\frac{a^2b^2}{a^2-b^2}\int_a^b \frac{\sin^2 R}{r^3}dr + b^2F\int_a^b \frac{\sin^2 R}{r}dr} \tag{71}$$

The terms dependant on D are negligible for the first two and problematic for the other two: they generate values many orders of magnitude too high. The nature of the problem is explained further in the discussion section. These terms will be neglected. The simplified expressions can then be written as

$$\Pi_{\text{nuc, simple, strain}} = \frac{\gamma_1 \ln\left(\frac{b}{a}\right)}{\left(\frac{b^2}{b^2-a^2}\right)\ln\left(\frac{b}{a}\right) + \frac{1}{2}} \tag{10}$$

$$\Pi_{\text{nuc, simple, stress}} = \frac{F\gamma_1 \ln\left(\frac{b}{a}\right)}{F\left(\frac{b^2}{b^2-a^2}\right)\ln\left(\frac{b}{a}\right) + \frac{1}{2}} \tag{11}$$

$$\Pi_{\text{nuc, radial, strain}} = \frac{\gamma_1\int_a^b \frac{\sin^2 R}{r}dr}{\frac{a^2b^2}{a^2-b^2}\int_a^b \frac{\sin^2 R}{r^3}dr + b^2\int_a^b \frac{\sin^2 R}{r}dr} \tag{12}$$

$$\Pi_{\text{nuc, radial, stress}} = \frac{\gamma_1 F\int_a^b \frac{\sin^2 R}{r}dr}{\frac{a^2b^2}{a^2-b^2}\int_a^b \frac{\sin^2 R}{r^3}dr + b^2F\int_a^b \frac{\sin^2 R}{r}dr} \tag{13}$$

after terms have been neglected.

It is then possible to find the gradient, $\frac{dn^2}{d\Pi}$, for Eq. 62-65. Since the resulting gradients are proportional to E^{-1} from expanding D_{strain} and D_{stress}, this gradient can be used to find the elastic modulus:

$$\frac{dn^2}{d\Pi} = \frac{-12(1-\nu^2)}{(E_{\text{simple, strain}})\,h^3}\left(\frac{a^2b^2}{a^2-b^2}\right)\left\{\frac{b^2\ln\left(\frac{b}{a}\right)}{b^2-a^2} + \frac{1}{2}\right\} \tag{72}$$

$$\frac{dn^2}{d\Pi} = \frac{-12}{(E_{\text{simple, stress}})h^3}\left(\frac{a^2b^2}{a^2-b^2}\right)\left\{\frac{b^2\ln\left(\frac{b}{a}\right)}{b^2-a^2}F + \frac{1}{2}\right\} \tag{73}$$

$$\frac{dn^2}{d\Pi} = \frac{-6(1-\nu^2)b^2}{(E_{\text{radial, strain}})h^3(a^2-b^2)}\left\{\frac{\int_a^b \frac{\sin^2 R}{r}dr}{\int_a^b \frac{\sin^2 R}{r^3}dr} + a^2\right\} \tag{74}$$

$$\frac{dn^2}{d\Pi} = \frac{-6b^2}{(E_{\text{radial, stress}})h^3(a^2-b^2)}\left\{\frac{\int_a^b \frac{\sin^2 R}{r}dr}{\int_a^b \frac{\sin^2 R}{r^3}dr} + a^2F\right\} \tag{75}$$

The rearrangement to make the elastic modulus the subject of the equation is then trivial and has the following results:

$$E_{\text{simple, strain}} = \frac{-12(1-\nu^2)}{\left(\frac{dn^2}{d\Pi}\right)h^3}\left(\frac{a^2b^2}{a^2-b^2}\right)\left\{\frac{b^2\ln\left(\frac{b}{a}\right)}{b^2-a^2}+\frac{1}{2}\right\} \tag{5}$$

$$E_{\text{simple, stress}} = \frac{-12}{\left(\frac{dn^2}{d\Pi}\right)h^3}\left(\frac{a^2b^2}{a^2-b^2}\right)\left\{\frac{b^2\ln\left(\frac{b}{a}\right)}{b^2-a^2}F+\frac{1}{2}\right\} \tag{6}$$

$$E_{\text{radial, strain}} = \frac{-6(1-\nu^2)b^2}{\left(\frac{dn^2}{d\Pi}\right)h^3(a^2-b^2)}\left\{\frac{\int_a^b \frac{\sin^2\left(\frac{\pi(r-a)}{(b-a)}\right)}{r}dr}{\int_a^b \frac{\sin^2\left(\frac{\pi(r-a)}{(b-a)}\right)}{r^3}dr}+a^2\right\} \tag{8}$$

$$E_{\text{radial, stress}} = \frac{-6b^2}{\left(\frac{dn^2}{d\Pi}\right)h^3(a^2-b^2)}\left\{\frac{\int_a^b \frac{\sin^2\left(\frac{\pi(r-a)}{(b-a)}\right)}{r}dr}{\int_a^b \frac{\sin^2\left(\frac{\pi(r-a)}{(b-a)}\right)}{r^3}dr}+a^2F\right\} \tag{9}$$

B Error Propagation Expressions

$$\delta E_{\text{simple,strain}} = E_{\text{simple,strain}} \times \left\{ \left(\frac{-24ab^4(\nu^2-1)}{Gh^3(b^2-a^2)^3}(b^2+a^2)\ln\left(\frac{b}{a}\right)\right)^2 (\delta a)^2 + \left(\frac{-24a^2b(1-\nu^2)}{Gh^3(a^2-b^2)}\left(\frac{b^2\ln\left(\frac{b}{a}\right)}{b^2-a^2}+\frac{1}{2}\right) + \frac{-24a^2b^3(1-\nu^2)}{Gh^2(b^2-a^2)^2}\left(\frac{b^2\ln\left(\frac{b}{a}\right)}{b^2-a^2}+\frac{1}{2}\right) + \frac{-12a^2b^3(1-\nu^2)}{b^2-a^2} + \frac{2b\ln\left(\frac{b}{a}\right)}{b^2-a^2} - \frac{2b^2\ln\left(\frac{b}{a}\right)}{Gh^3(a^2-b^2)^3}\right)^2 (\delta b)^2 + \left(\frac{-6a^2b^2(\nu^2-1)}{h^2g^2(a^2-b^2)^2}\left(a^2-2b^2\ln\left(\frac{b}{a}\right)-b^2\right)\right)^2 (\delta G)^2 + \left(\left(\frac{-18a^2b^2(\nu^2-1)}{Gh^4(a^2-b^2)^2}\right)(a^2-2b^2\ln\left(\frac{b}{a}\right)-b^2)\right)^2 (\delta h)^2 \right\}^{\frac{1}{2}} \quad (76)$$

$$\delta E_{\text{simple,stress}} = _{\text{simple,strain}} \times \left\{ \left(\frac{-24ab^4(\nu^2-1)}{Gh^3(b^2-a^2)^3}(b^2+a^2)F\ln\left(\frac{b}{a}\right)\right)^2 (\delta a)^2 + \left(\frac{-24a^2b(1-\nu^2)}{Gh^3(a^2-b^2)}\left(\frac{b^2F\ln\left(\frac{b}{a}\right)}{b^2-a^2}+\frac{1}{2}\right) + \frac{-24a^2b^3(1-\nu^2)}{Gh^2(b^2-a^2)^2}\left(\frac{b^2F\ln\left(\frac{b}{a}\right)}{b^2-a^2}+\frac{1}{2}\right) + \frac{-12a^2b^3(1-\nu^2)}{b^2-a^2} + \frac{2bF\ln\left(\frac{b}{a}\right)}{b^2-a^2} - \frac{2b^2F\ln\left(\frac{b}{a}\right)}{Gh^3(a^2-b^2)^3}\right)^2 (\delta b)^2 + \left(\frac{-6a^2b^2(\nu^2-1)}{h^2g^2(a^2-b^2)^2}\left(a^2-2b^2F\ln\left(\frac{b}{a}\right)-Fb^2\right)\right)^2 (\delta G)^2 + \left(\left(\frac{-18a^2b^2(\nu^2-1)}{Gh^4(a^2-b^2)^2}\right)(a^2-2b^2F\ln\left(\frac{b}{a}\right)-Fb^2)\right)^2 (\delta h)^2 \right\}^{\frac{1}{2}} F \quad (77)$$

$$\delta E_{\text{radial,strain}} = E_{\text{radial, strain}} \times \left\{ \left(\frac{-3}{h}\right)^2 (\delta h)^2 + \left(\frac{-1}{G}\right)^2 (\delta G)^2 + \left[\left(\frac{a^2-b^2}{b^2}\right) \times ... \sqrt{\left(\frac{-2ab^2}{a^2-b^2}\right)^2 (\delta a)^2 + \left(\frac{2a^2b(\delta b)^2}{(a^2-b^2)^2}\right)(\delta b)^2} \right]^2 + \left[\left(\frac{\delta Q}{Q}+\frac{\delta W}{W}\right)\frac{Q}{W} + \frac{2a(\delta a)}{\frac{Q}{W}+a^2} \right]^2 \right\}^{\frac{1}{2}} \quad (78)$$

$$\delta E_{\text{radial,stress}} = E_{\text{radial, stress}} \times \left\{ \left(\frac{-3}{h}\right)^2 (\delta h)^2 + \left(\frac{-1}{G}\right)^2 (\delta G)^2 + \left(\left(\frac{a^2-b^2}{b^2}\right) \times ... \sqrt{\left(\frac{-2ab^2}{a^2-b^2}\right)^2 (\delta a)^2 + \left(\frac{2a^2b(\delta b)^2}{(a^2-b^2)^2}\right)(\delta b)^2} \right)^2 + \left(\left(\frac{\delta Q}{Q}+\frac{\delta W}{W}\right)\frac{Q}{W} + \frac{2aF(\delta a)}{\frac{Q}{W}+a^2} \right)^2 \right\}^{\frac{1}{2}} \quad (79)$$

The δ symbol represents uncertainty on the following parameter. G represents the gradient $\frac{dn^2}{d\pi}$. Shorthand expressions have been used for the integrals:

$$Q \equiv \frac{\int_a^b \sin^2(R)dr}{r}$$

and

$$W \equiv \frac{\int_a^b \sin^2(R)dr}{r^3}$$

C Plots Used to Calculate Elastic Modulus Values

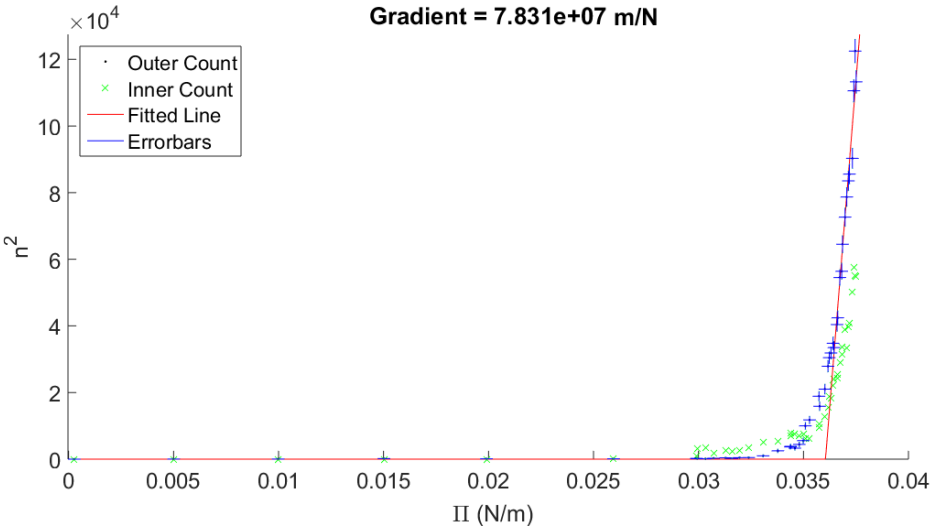

Figure 15: Results for dataset number 1 which used an annulus with $a = 4.9 \pm 0.1$ mm, $b = 10.6 \pm 0.15$ mm and $h = 82 \pm 2$ nm.

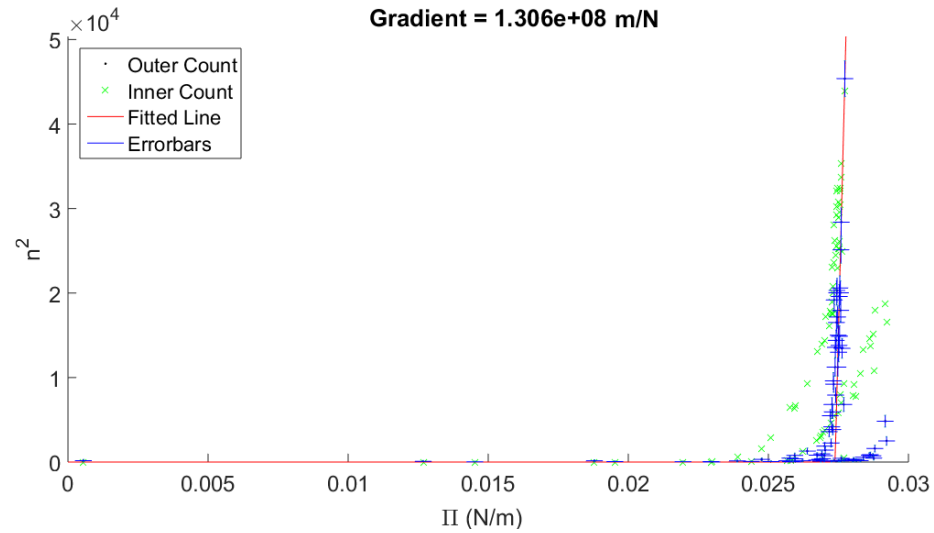

Figure 16: Results for dataset number 2 which used an annulus with $a = 5.9 \pm 0.1$ mm, $b = 10.4 \pm 0.15$ mm and $h = 82 \pm 2$ nm. The anomalous points at higher pressures are from images taken before overflowing and the others are taken after. It can be seen that the overflow reduced the measured nucleation pressure significantly but the gradient was still extracted. The effect this has on γ_1 makes the measured elastic modulus incorrect. The result was included for completeness.

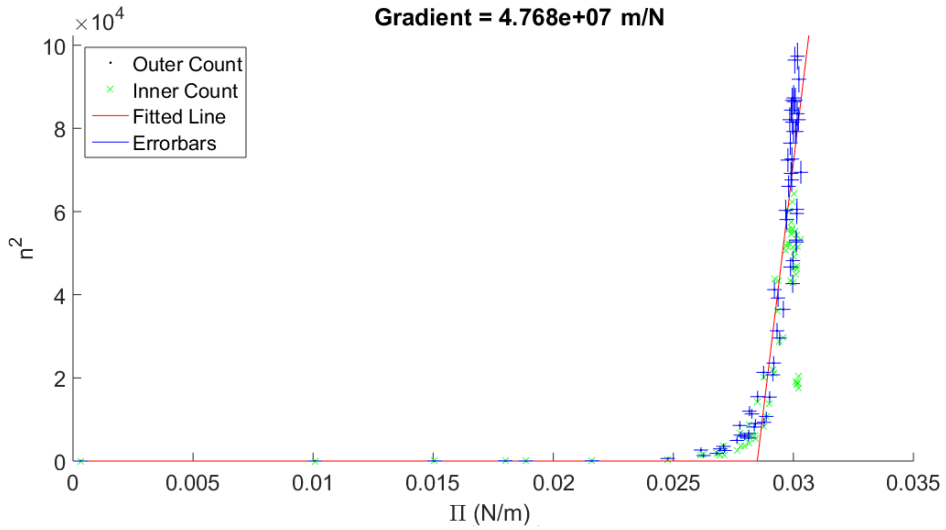

Figure 17: Results for dataset number 3 which used an annulus with $a = 5.7 \pm 0.1$ mm, $b = 10.6 \pm 0.15$ mm and $h = 82 \pm 2$ nm.

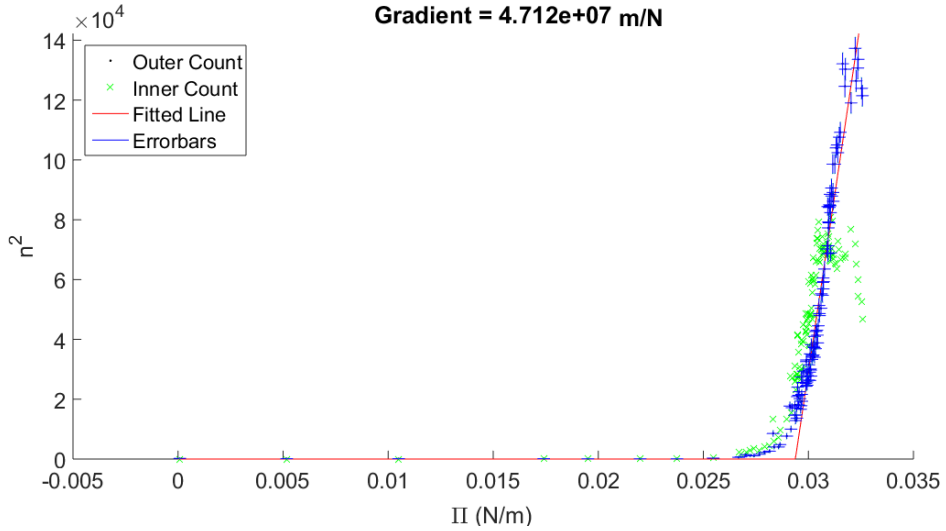

Figure 18: Results for dataset number 4 which used an annulus with $a = 5.1 \pm 0.1$ mm, $b = 10.1 \pm 0.2$ mm and $h = 82 \pm 2$ nm.

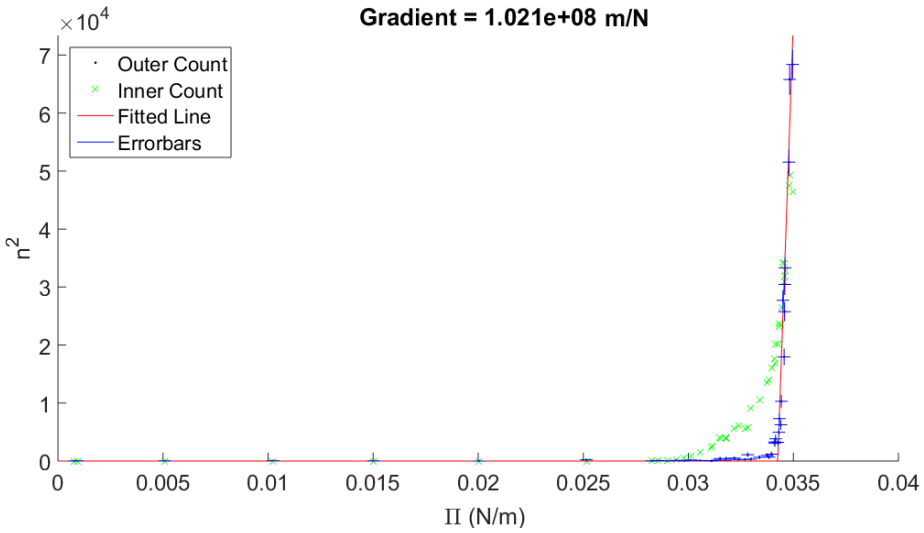

Figure 19: Results for dataset number 5 which used an annulus with $a = 5.6 \pm 0.1$ mm, $b = 10.3 \pm 0.2$ mm and $h = 82 \pm 2$ nm.

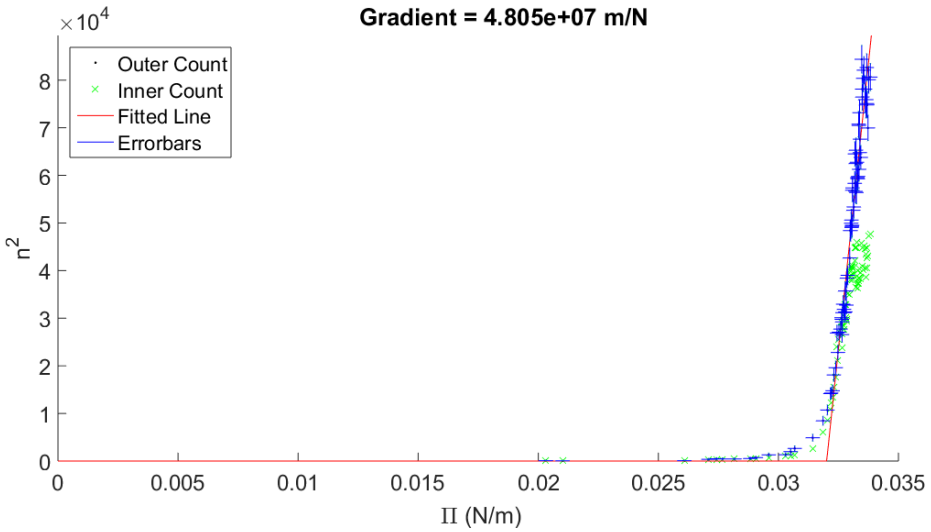

Figure 20: Results for dataset number 6 which used an annulus with $a = 4.6 \pm 0.1$ mm, $b = 9.5 \pm 0.2$ mm and $h = 82 \pm 2$ nm.

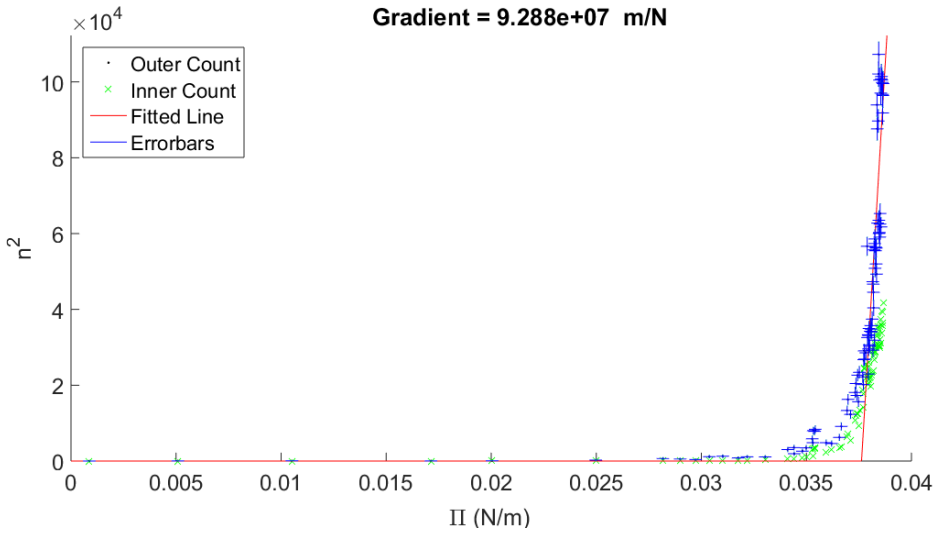

Figure 21: Results for dataset number 7 which used an annulus with $a = 4.2 \pm 0.1$ mm, $b = 9.7 \pm 0.2$ mm and $h = 91 \pm 5$ nm.

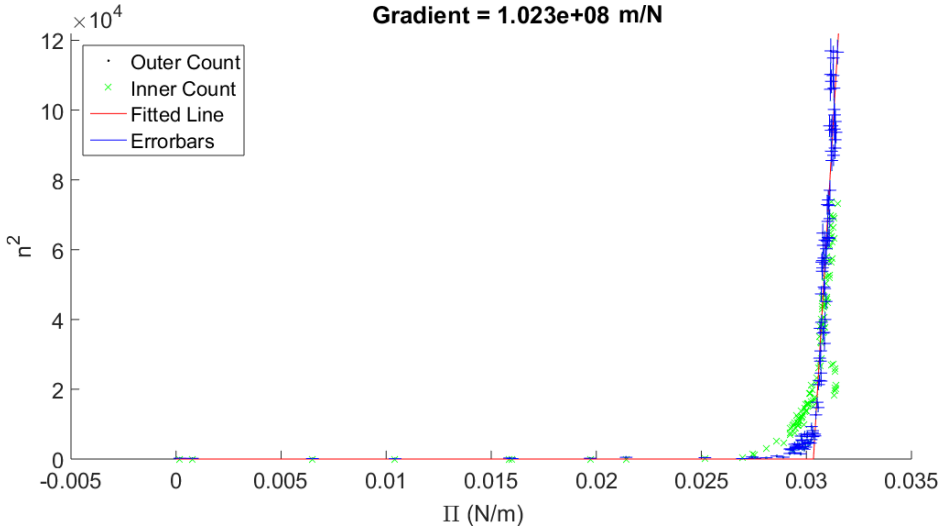

Figure 22: Results for dataset number 8 which used an annulus with $a = 6.0 \pm 0.1$ mm, $b = 10.8 \pm 0.2$ mm and $h = 91 \pm 5$ nm.

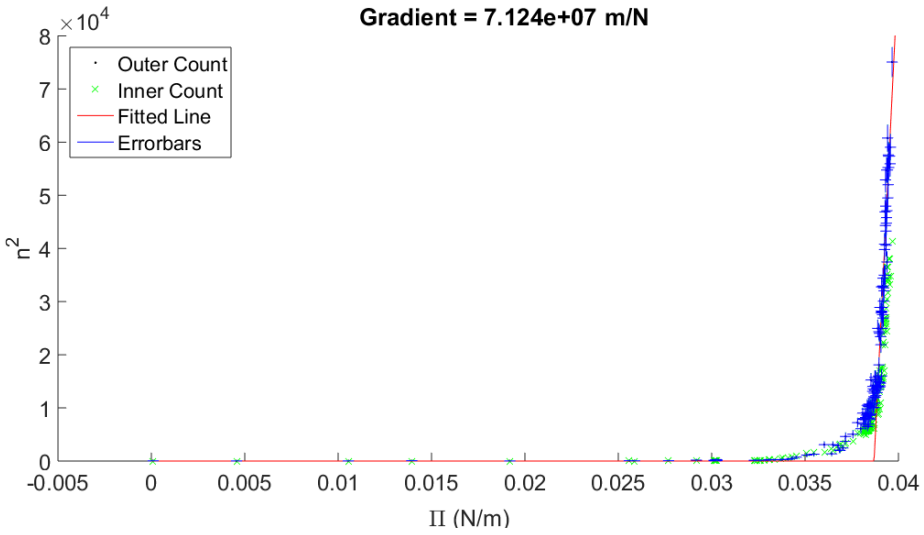

Figure 23: Results for dataset number 9 which used an annulus with $a = 3.8 \pm 0.1$ mm, $b = 7.7 \pm 0.2$ mm and $h = 80 \pm 2$ nm.

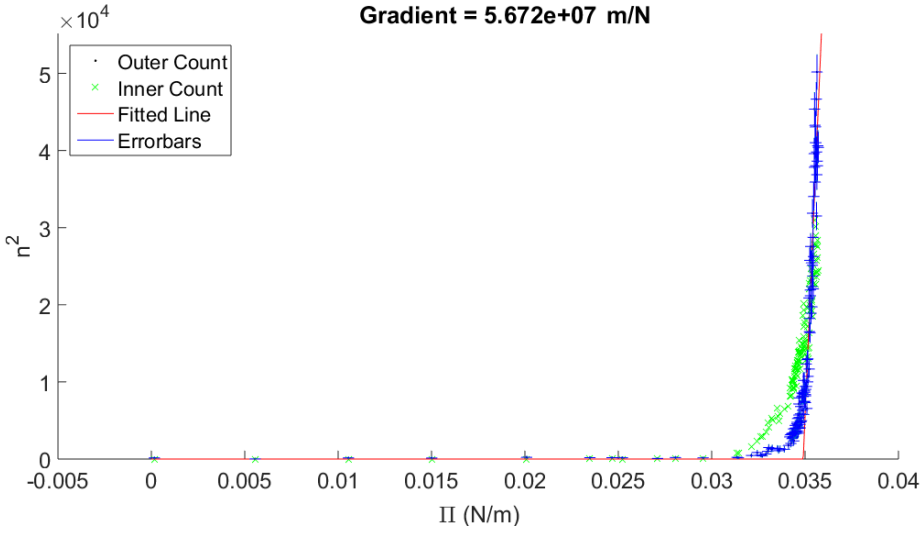

Figure 24: Results for dataset number 10 which used an annulus with $a = 3.9 \pm 0.1$ mm, $b = 9.0 \pm 0.2$ mm and $h = 80 \pm 2$ nm.

D Image Analysis MATLAB Code

```
clear, close all;

%% Predefining parameters
% sets font size of figures
set(0,'defaultAxesFontSize', 18)

% Controls the circle detection
inSens = 0.90;
outSens = 0.95;
edge = 0.1;
threshold = 15;
peakthreshold = 0.5;

% The size of a pixel in real space meters is
conversion = 1.52e-05;

% Defines the colour spaces for the area calculation and original colour
% displaying of images
RGBColourArray = linspace(0,1,120)';
RGBMap = [RGBColourArray, RGBColourArray, RGBColourArray];
mask =  [0, 0, 0; 1, 1, 1];
invMask = [1, 1, 1; 0, 0, 0];

%% Load the images and remove the background
% Need to ensure that the first .tiff file is the background alphabetically

% loads the file names and opens the background separately to the rest
% (also sorts them alphabetically/by surface pressure)
path = uigetdir('','Please identify the folder of images');
oldFolder = cd(path);
imageFiles = dir('*.tiff');
imageFiles = sort({imageFiles.name});
nFiles = length(imageFiles);
nImages = nFiles-1;
backgroundImage = imread(imageFiles{1});
[pathstr,folderName,ext] = fileparts(path);

% defines empty arrays for the images and other variables
images = cell(1,nImages);
RGBImages = cell(1,nImages);
smallCenters = zeros(2,nImages);
bigCenters = zeros(2,nImages);
smallRadii = zeros(1,nImages);
bigRadii = zeros(1,nImages);
sigmas = zeros(1,nImages);

% loads the rest of the images into a cell array called "images" and
% finds the values of surface pressure in mN/m and stores them in an array
for file=2:nFiles % accounts for background
    imageName = imageFiles{file};
    images{file-1} = imread(imageName) - backgroundImage;
    sigmaIndex = strfind(imageName, '=');
    sigmaString = imageName(sigmaIndex+2:end-5);
    if sigmaString(1) == '-';
        sigmaString(1) = '0';
    end
```

```
57      sigmas(file-1) = str2double(strrep(sigmaString, '-','.'));
58  end
59
60  cd(oldFolder) % returns user to code folder
61  disp('Images loaded successfully...')
62
63  %% find the circles using bwconncomp method using the mask colormaps
64
65  for i=1:nImages;
66      % loads the image and thresholds it to eliminate shadows and noise.
67      % the images are then converted to dinary images and one has a light
68      % annulus on a black background and one has a dark annulus on a light
69      % background, so that the bwconncomp function can find the annulus and
70      % missing circle.
71      beforeImage = images{i};
72      beforeImage(beforeImage<threshold) = 0;
73      annulusImage = ind2rgb(beforeImage, mask);
74      annulusImage = annulusImage(:,:,1);
75      innerImage = ind2rgb(beforeImage, invMask);
76      innerImage = innerImage(:,:,1);
77
78      % finds the indeces of the annulus in the image by selecting the
79      % longest array of indeces and calculates the area as the number of
80      % pixels
81      CC = bwconncomp(annulusImage, 6);
82      throwCell1 = CC.PixelIdxList;
83      sizes = cellfun(@size,throwCell1,'uniform',false);
84      [trash, indeces]=sortrows(cat(1,sizes{:}),-[1 2]);
85      throwCell1 = throwCell1(indeces);
86      annulusIndeces = throwCell1{1};
87      annulusArea = length(throwCell1{1});
88
89      % does the same but takes the second biggest as the biggest is the
90      % background outside of the annulus.
91      CC2 = bwconncomp(innerImage, 6);
92      throwCell2 = CC2.PixelIdxList;
93      sizes = cellfun(@size,throwCell2,'uniform',false);
94      [trash, indeces]=sortrows(cat(1,sizes{:}),-[1 2]);
95      throwCell2 = throwCell2(indeces);
96      innerIndeces = throwCell2{2};
97      innerArea = length(innerIndeces);
98
99      % converts the areas to radii
100     smallRadii(i) = round(sqrt(innerArea / pi))-10;
101     bigRadii(i) = round(sqrt((annulusArea + innerArea)/pi))-10;
102
103     % converts the index values to x and y values and then means them to
104     % find the center for each
105     [bigY, bigX] = ind2sub([1940,2588], annulusIndeces);
106     bigCenters(:, i) = [round(mean(bigX)), round(mean(bigY))];
107     [smallY, smallX] = ind2sub([1940,2588], innerIndeces);
108     smallCenters(:, i) = [round(mean(smallX)), round(mean(smallY))];
109 end
110
111 disp('Circles found...');
112
113 %% Finds the size of the circles for use in calculating E
114 % Applies threshold and gaussian blur onto unwrinkled annulus image to get
```

```
115 % more accurate and precise value of a and b
116
117 % uses imfindcirces to find a more accurate measure of the radii
118 thresholdImage = images{1};
119 thresholdImage(thresholdImage<threshold) = 0;
120 maskedImage = imgaussfilt(ind2rgb(thresholdImage, mask), 5);
121 smallRange = [smallRadii(1) - 20, smallRadii(1)+10];
122 bigRange = [bigRadii(1) - 20, bigRadii(1)+10];
123
124 [smallCenter, a] = imfindcircles(maskedImage,...
125 smallRange, 'Sensitivity', inSens, 'EdgeThreshold', edge,...
126 'ObjectPolarity', 'dark');
127
128 [bigCenter, b] = imfindcircles(maskedImage,bigRange,...
129     'Sensitivity', outSens, 'EdgeThreshold', edge, 'ObjectPolarity',...
130     'bright');
131
132 a = a.*conversion;
133 b = b.*conversion;
134 disp(['Radius estimates found as: ', num2str(b.*1000), 'mm and ', num2str(a
    .*1000), 'mm'])
135
136 %% Take the profile at fixed theta with increasing radius to try and
    measure the shape of the radial bending
137
138 % The full profile output is the intensity at each point in the annulus.
139 % The radial profile is the average of these, averages over the values of
140 % theta so that the average intensity of the wrinkles (bright and dark) can
141 % be found. The tangential profile averages for each value of R and
142 % so is the average intesity over each circular intensity profile.
143 % Tangential profile is used to count wrinkles while radial profile is used
144 % to determine the shape of the radial bending.
145
146 radialProfile = cell(1,nImages);
147 innerTangentialProfile = cell(1,nImages);
148 outerTangentialProfile = cell(1,nImages);
149 fullProfile = cell(1,nImages);
150 n1 = zeros(1,nImages);
151 n2 = zeros(1,nImages);
152 trim = 10; % this reduces a and b to not consider any black pixels from
    over estimation
153
154 for i = 1:nImages
155     tempImage = (images{i});
156     % all values of theta possible arond the outer radius (no. of pixels
157     % in diameter is no. of theta values. A similar thing is done for the
158     % values of radius.
159     theta = 0:1/bigRadii(i):2*pi;
160     radialValues = smallRadii(i)+trim:1:bigRadii(i)-trim; % 0.5*(bigRadii(i
        ) + smallRadii(i));
161     radialIntensity = zeros(length(radialValues),1);
162     tempProfile = zeros(length(theta),length(radialValues));
163     % double loop so that all pixels inside the annulus are considered
164     for j = 1:length(radialValues)
165         x = round(radialValues(j) .* cos(theta) + bigCenters(2,i));
166         y = round(radialValues(j) .* sin(theta) + bigCenters(1,i));
167         for k = 1:length(theta)
168             radialIntensity(k) = (tempImage(x(k),y(k)));
```

```
169             end
170             tempProfile(:,j) = radialIntensity;
171         end
172         fullProfile{i} = (tempProfile);
173         radialProfile{i} = mean(tempProfile,1);
174         innerTangentialProfile{i} = mean(tempProfile(:,1:floor(length(
                radialValues./2))),2);
175         outerTangentialProfile{i} = mean(tempProfile(:,floor(length(
                radialValues./2)):end),2);
176         % find peaks can be thresholded by finding the indeces for which the
177         % peak prominence is too small. The peaks and troughs are counted and
178         % the mean is used
179         peaks1 = findpeaks((innerTangentialProfile{i}),'MinPeakProminence',5,
                ...
180             'MaxPeakWidth', 30);
181         peaks2 = findpeaks((-innerTangentialProfile{i}),'MinPeakProminence',5,
                ...
182             'MaxPeakWidth', 30);
183         n1(i) = 0.5.*(length(peaks1)+length(peaks2));
184         peaks1 = findpeaks((outerTangentialProfile{i}),'MinPeakProminence',10,
                ...
185             'MaxPeakWidth', 30);
186         peaks2 = findpeaks((-outerTangentialProfile{i}),'MinPeakProminence',10,
                ...
187             'MaxPeakWidth', 30);
188         n2(i) = 0.5.*(length(peaks1)+length(peaks2));
189 end
190
191 disp('Peaks counted...');
192
193
194 %% Calculates the Elastic Modulus for the sample and plots graph
195
196 % declare variables/reminder of the variables used
197 r = linspace(a, b, 1000);
198 v = 0.325; %poisson ratio - needs reference
199 gamma1 = 0.0725; %surface tension of water - needs reference
200 Pi = sigmas*10^-3;
201
202 thicknesses = [80, 83, 82, 91].*10^-9; % determined by ellipsometry results
203 % thickness 1: 80 +/- 2
204 % thickness 2: 83 +/- 7
205 % thickness 3: 82 +/- 2
206 % thickness 4: 91 +/- 5
207 h = thicknesses(str2num(path(strfind(path,'thickness')+9)));
208
209 % variables and shorthands
210 A = a.^2 - b.^2;
211 nucPi2 = (-A.*gamma1.*log(b./a))./(b.^2 .* log(b./a) + ((-A)./2));
212 S = sin(pi.*(r - a)./(b-a));
213 nsq1 = n1.^2;
214 nsq2 = n2.^2;
215 PiErr = 0.0003.*ones(1,nImages);
216 nsqErr = (10./n2).*nsq2;
217
218 % selects the linear region of n^2 values - values above linearCutoff.
219 % Change this parameter to fit to linear region
220 linearThreshold = 160;
```

```
221 usedN = n2(n2>linearThreshold);
222 usedNsq = usedN.^2;
223 usedPi = Pi(n2>linearThreshold);
224 [fit, errors] = polyfit(usedPi, usedNsq, 1);
225 gradient = fit(1);
226 intercept = fit(2);
227
228 % fits linear section
229 fitPi = linspace(0,max(Pi)+0.001, 1000);
230 fittedline = gradient.*fitPi + intercept;
231 foundNuc = -intercept./gradient;
232 fittedline(fittedline<0) = 0;
233
234 % Plots stuff
235 figure
236 hold on
237 plot(Pi, nsq2, 'k.')
238 plot(Pi, nsq1,'gx');
239 plot(fitPi, fittedline, 'r-')
240 hold off
241 xyerrorbar(Pi, nsq2, PiErr, nsqErr); %contains hold on and off in the
      function
242 xlabel('Pi')
243 ylabel('n^2')
244 ylim([0,max(nsq2)+5000])
245 legend('Outer Count', 'Inner Count', 'Fitted Line', 'Errorbars', 'Location'
      , 'NW')
246 title(['Gradient = ', num2str(gradient,'%.3e')])
247
248 %% Elastic Modulus values
249
250 % simple strain value of R
251 oldE = -12.*(1-v.^2)./(gradient.*h.^3) .*(a.^2.*b.^2 ./A) .*(b.^2./(-A).*
      log(b./a) + 0.5)
252
253 % radial strain value of E
254 newE = -6.*(1-v.^2).*b.^2./(gradient.*h.^3 .* A) .* (trapz(S.^2./r)./trapz(
      S.^2./r.^3) + a.^2);
255
256 % These are the expressions after converting the plain strain problem into
      plain stress
257 stress1 = 1-(v ./ (1+v)).^2;
258 stress2 = v./(1-2.*v);
259 stress3 = a.^2 .*( ( 2 .* stress2) + 2 ./ (stress2 + 1) -1./(stress2 + 0.5)
      );
260 stressPref = -6.* (stress1).* (1+v).^2 .* b.^2 ./ (gradient .* h.^3 .*
      (1+2.*v).*A);
261
262 % simple stress value of E
263 stressNoRadialE = -12.*stress1.*(1+v).^2./(gradient.*h.^3.*(1+2.*v)) .*(a
      .^2.*b.^2 ./A) .*(b.^2./(-A).*log(b./a).*( ( 2 .* stress2) + 2 ./ (
      stress2 + 1) - 1./(stress2 + 0.5)) + 1/2)
264
265 % radial stress value of E
266 stressRadialE = stressPref.*(trapz(S.^2/r)./trapz(S.^2./r.^3) + stress3)
267
268 %% saves the results
269
```

```
saveName = path(strfind(path, '\17')+1 : end);
savePath = [path(1:strfind(path, '\Image')), 'outputs\', saveName, '.mat'];
save(savePath, 'n1', 'n2', 'Pi', 'gradient', 'intercept', 'oldE', 'newE', '
    stressRadialE', 'stressNoRadialE', 'h', 'a', 'b', 'PiNuc', '
    linearThreshold');
disp('Results saved...')

% Audible notification of completion. The script takes several minutes to
% run.
beep
```